



Ataxin-3 Links NOD2 and TLR2 Mediated Innate Immune Sensing and Metabolism in Myeloid Cells

Thomas P. Chapman^{1†}, Daniele Corridoni^{1†}, Seiji Shiraishi¹, Sumeet Pandey², Anna Aulicino¹, Simon Wigfield³, Maria do Carmo Costa⁴, Marie-Laëtizia Thézénas⁵, Henry Paulson⁴, Roman Fischer⁵, Benedikt M. Kessler⁵ and Alison Simmons^{1*}

¹ MRC Human Immunology Unit, MRC Weatherall Institute of Molecular Medicine, John Radcliffe Hospital, University of Oxford, Oxford, United Kingdom, ² Translational Gastroenterology Unit, John Radcliffe Hospital, University of Oxford, Oxford, United Kingdom, ³ Department of Oncology, University of Oxford, Oxford, United Kingdom, ⁴ Department of Neurology, University of Michigan, Ann Arbor, MI, United States, ⁵ Nuffield Department of Medicine, Target Discovery Institute, University of Oxford, Oxford, United Kingdom

OPEN ACCESS

Edited by:

Hannes Stockinger,
Medical University of Vienna, Austria

Reviewed by:

Jaya Talreja,
Wayne State University, United States
Guntram A. Grassl,
Hannover Medical School, Germany

*Correspondence:

Alison Simmons
alison.simmons@imm.ox.ac.uk

[†]These authors have contributed
equally to this work

Specialty section:

This article was submitted to
Molecular Innate Immunity,
a section of the journal
Frontiers in Immunology

Received: 02 April 2019

Accepted: 14 June 2019

Published: 19 July 2019

Citation:

Chapman TP, Corridoni D, Shiraishi S, Pandey S, Aulicino A, Wigfield S, do Carmo Costa M, Thézénas M-L, Paulson H, Fischer R, Kessler BM and Simmons A (2019) Ataxin-3 Links NOD2 and TLR2 Mediated Innate Immune Sensing and Metabolism in Myeloid Cells. *Front. Immunol.* 10:1495. doi: 10.3389/fimmu.2019.01495

The interplay between NOD2 and TLR2 following recognition of components of the bacterial cell wall peptidoglycan is well-established, however their role in redirecting metabolic pathways in myeloid cells to degrade pathogens and mount antigen presentation remains unclear. We show NOD2 and TLR2 mediate phosphorylation of the deubiquitinase ataxin-3 via RIPK2 and TBK1. In myeloid cells ataxin-3 associates with the mitochondrial cristae protein MIC60, and is required for oxidative phosphorylation. Depletion of ataxin-3 leads to impaired induction of mitochondrial reactive oxygen species (mROS) and defective bacterial killing. A mass spectrometry analysis of NOD2/TLR2 triggered ataxin-3 deubiquitination targets revealed immunometabolic regulators, including HIF-1 α and LAMTOR1 that may contribute to these effects. Thus, we define how ataxin-3 plays an essential role in NOD2 and TLR2 sensing and effector functions in myeloid cells.

Keywords: Nod2, TLR2, metabolism, innate immunity, ataxin 3

INTRODUCTION

Pattern recognition receptors (PRRs) recognize foreign antigen to direct innate and adaptive immune responses against invading pathogens (1). Polymorphisms in the PRR nucleotide-binding oligomerization domain-containing protein 2 (NOD2) represent the strongest genetic risk factor for the inflammatory bowel disease Crohn's (CD), and thus this bacterial sensor is the focus of particular research interest (2–4). NOD2 recognizes muramyl dipeptide (MDP), the largest fraction of peptidoglycan, that is present in the cell walls of all bacteria (5). Subsequent activation of NF- κ B and MAPK pathways via interaction with receptor-interacting protein kinase 2 (RIPK2) results in an array of immune responses, such as production and regulation of pro-inflammatory cytokines (6), and modulation of T-cell function (7–9). NOD2 also directs autophagy, which is important both for bacterial clearance and MHC class II antigen presentation (10). Importantly, NOD2 signaling is intimately linked with that of toll like receptor TLR2, with both responding to ligands derived from the same bacterial component, peptidoglycan. Although the precise mechanisms of cross-regulation are not well-understood, both NOD2 and TLR2 activate separate upstream signaling cascades to recruit the same NF- κ B and MAPK pathways, and are typically thought to act in a synergistic fashion (11). CD patients harboring NOD2 polymorphisms display loss-of-function for induction of NOD2

and NOD2/TLR2 effector signaling factors (12, 13). In contrast, gain-of-function mutations of NOD2 have been associated with other inflammatory disease, such as Blau syndrome and early-onset-sarcoidosis (EOS).

In recent years it has become clear that cross-talk between metabolic and immune pathways is central to the regulation of host defense (14). Immune cells undergo significant metabolic reprogramming during the immune response, both as a result of changes in the metabolic microenvironment induced by inflammation, and in response to immune triggering. This interplay appears of particular importance to dendritic cells and macrophages and controls core processes including differentiation (15). However, while the importance of PRR activation in directing metabolic pathways that impact on immune effector function is now well-established, how NOD2 and TLR2 influence myeloid metabolism is unclear. Here, following a phosphoproteomic screen of NOD2 and TLR signaling we identify a deubiquitinase essential for metabolic reprogramming and innate effector function in myeloid cells.

RESULTS

NOD2 and TLR2 Stimulation Leads to Ataxin-3 Phosphorylation Mediated by RIPK2 and TBK1

We identified ataxin-3 as one of the most differentially phosphorylated proteins on NOD2/TLR2 stimulation through a quantitative phosphoproteomic screen in monocyte derived dendritic cells (moDCs) from healthy human donors (**Supplementary Table 1**). Ataxin-3 is a deubiquitinase (DUB) (16) that is required for non-selective autophagy and that is linked to neurodegenerative disease (17–19).

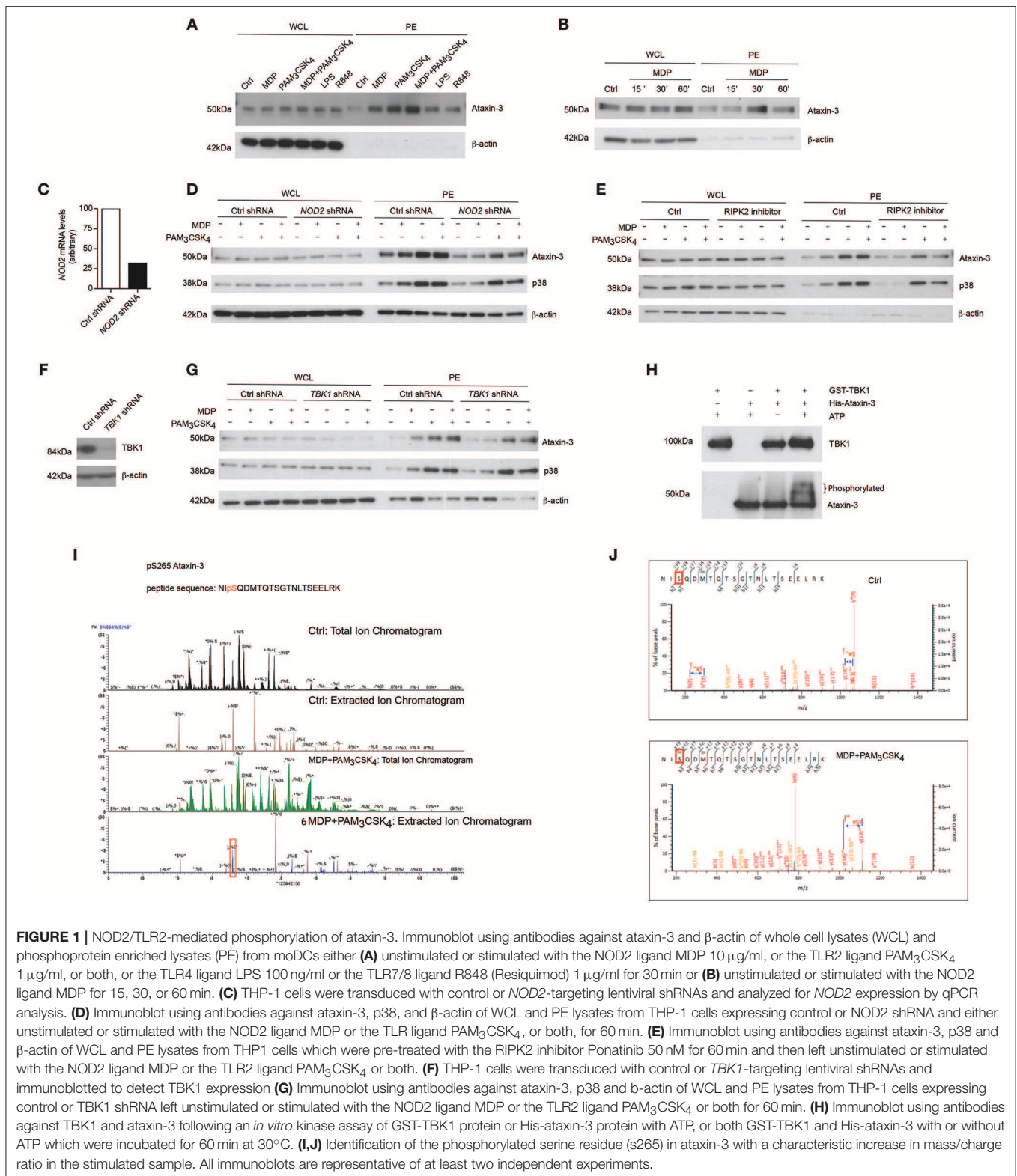
We first validated this result by immunoblotting phospho-enriched samples for ataxin-3 (**Figure 1A**). Both NOD2 and TLR2 stimulation alone led to ataxin-3 phosphorylation; this effect was enhanced on dual stimulation of NOD2 and TLR2. It was also observed to a lesser extent following stimulation of TLR4, TLR7, and TLR8 (**Figure 1A**). NOD2 mediated phosphorylation of ataxin-3 was examined in greater detail. A time course experiment demonstrated that ataxin-3 phosphorylation was maximal 30 min after MDP stimulation (**Figure 1B**). While NOD2 is the only known receptor for MDP, the absolute requirement for NOD2 in the MDP stimulated phosphorylation of ataxin-3 was investigated. We downregulated expression of NOD2 in THP-1 cells using short hairpin RNAs (shRNA) targeting *NOD2* (**Figure 1C**). Reduction of ataxin-3 phosphorylation on MDP exposure was observed in NOD2 knockdown cells (**Figure 1D**). Next, given the central importance of RIPK2 in NOD2 signaling (20, 21), the requirement of RIPK2 for phosphorylation of ataxin-3 by NOD2 was investigated. NOD2-RIPK2 inflammatory signaling can be potently and selectively inhibited by the clinically relevant kinase inhibitor Ponatinib, that functions by blocking RIPK2 autophosphorylation and ubiquitination (22). moDCs were treated with Ponatinib prior to stimulation with MDP or PAM₃CSK₄ or both, with phosphorylation of p38 used as

a positive control for the inhibitor. As expected, inhibition of RIPK2 blocked NOD2 induced phosphorylation of p38, but had no effect on induction by TLR2, which signals to p38 via a MyD88 pathway which is independent of RIPK2 (23). Inhibition of RIPK2 led to complete inhibition of NOD2 induced phosphorylation of ataxin-3, and significant abrogation of the synergistic NOD2/TLR2 signal in both cell types (**Figure 1E**). Recent evidence suggests that tank binding kinase 1 (TBK1) may represent a novel but important kinase in the NOD2/RIPK2 signaling cascade (24, 25) and MDP stimulation of the NOD2 receptor has been shown to induce TBK1 phosphorylation at S172 (24). Consequently, the requirement for TBK1 in NOD2/RIPK2 dependent phosphorylation of ataxin-3 was examined. We downregulated expression of TBK1 in THP-1 cells using short hairpin RNAs (shRNA) targeting *TBK1* (**Figure 1F**). Reduction of ataxin-3 phosphorylation on MDP exposure was observed in TBK1 knockdown cells (**Figure 1G**). The possibility that TBK1 might directly phosphorylate ataxin-3, as has been described for a number of other proteins including optineurin (26) and p62 (27), was explored using an *in vitro* kinase assay (**Figure 1H**). The expected autophosphorylation of TBK1 was demonstrated by a marginally higher molecular weight of the TBK1 band in samples containing both TBK1 and ATP. Importantly, a significant proportion of the ataxin-3 band was noted at a higher molecular weight in samples containing ataxin-3, TBK1 and ATP, consistent with ataxin-3 phosphorylation (**Figure 1H**). Notably, no change in migration of the ataxin-3 band was seen in samples containing ataxin-3 and TBK1 but not ATP, confirming the ATP dependency of this shift, consistent with phosphorylation. Finally, the phosphorylation site of ataxin-3 was sought, using liquid chromatography mass spectrometry analysis of endogenous ataxin-3 immunoprecipitated from THP-1 cells. A significant shift in mass/charge ratio, consistent with phosphorylation, was detected at a single peptide in the MDP/PAM₃CSK₄ stimulated sample only, corresponding to phosphorylation at serine 265 (**Figure 1I**). This residue has been described as a phosphorylation site in 12 separate large scale mass spectrometry (MS) screens of human primary cells and cell lines (28), and is highly conserved in placental bearing mammals (29), but there is no existing knowledge of its functional relevance. It is located in close proximity to the second ubiquitin interacting motif (UIM), suggesting that phosphorylation could affect specificity of DUB target, as has been described for neighboring serine residues 256/260/261 (30) (**Figure 1J**).

Taken together, this data shows that activation of NOD2/TLR2 signaling pathway induces phosphorylation of the DUB ataxin-3. TBK1 is required for the direct phosphorylation of ataxin-3 at serine 265 following NOD2/TLR2 activation.

Ataxin-3 Localizes With the Mitochondrial Cristae Protein MIC60 and Regulates the Expression of the Oxphos Machinery Components

To identify novel interacting partners of ataxin-3 in innate immune cells, endogenous ataxin-3 was immunoprecipitated in moDCs from healthy human donors, and subjected to mass



spectrometry analysis. One of the most abundant proteins identified in the pull down was the mitochondrial cristae protein MIC60 (Figures 2A,B). The association between ataxin-3 and MIC60 was validated through immunoblot of

immunoprecipitated ataxin-3 (Figure 2C). There appeared to be no change in abundance of MIC60 when moDCs were stimulated with MDP + PAM₃CSK₄ prior to immunoprecipitation of ataxin-3, suggesting that NOD2/TLR2 stimulation does not

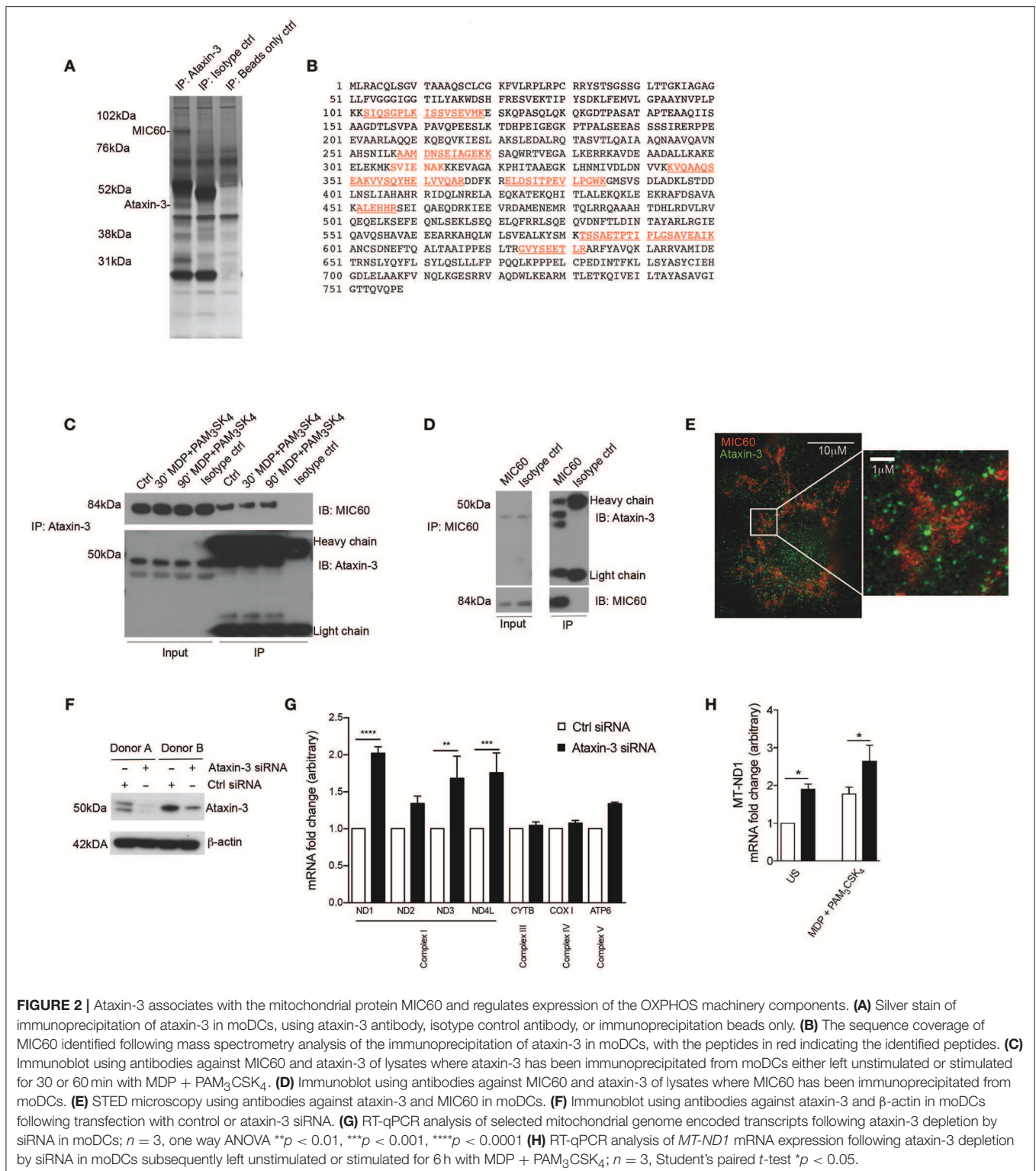


FIGURE 2 | Ataxin-3 associates with the mitochondrial protein MIC60 and regulates expression of the OXPHOS machinery components. **(A)** Silver stain of immunoprecipitation of ataxin-3 in moDCs, using ataxin-3 antibody, isotype control antibody, or immunoprecipitation beads only. **(B)** The sequence coverage of MIC60 identified following mass spectrometry analysis of the immunoprecipitation of ataxin-3 in moDCs, with the peptides in red indicating the identified peptides. **(C)** Immunoblot using antibodies against MIC60 and ataxin-3 of lysates where ataxin-3 has been immunoprecipitated from moDCs either left unstimulated or stimulated for 30 or 60 min with MDP + PAM₃CSK₄. **(D)** Immunoblot using antibodies against MIC60 and ataxin-3 of lysates where MIC60 has been immunoprecipitated from moDCs. **(E)** STED microscopy using antibodies against ataxin-3 and MIC60 in moDCs. **(F)** Immunoblot using antibodies against ataxin-3 and β -actin in moDCs following transfection with control or ataxin-3 siRNA. **(G)** RT-qPCR analysis of selected mitochondrial genome encoded transcripts following ataxin-3 depletion by siRNA in moDCs; $n = 3$, one way ANOVA $**p < 0.01$, $***p < 0.001$, $****p < 0.0001$ **(H)** RT-qPCR analysis of *MT-ND1* mRNA expression following ataxin-3 depletion by siRNA in moDCs subsequently left unstimulated or stimulated for 6 h with MDP + PAM₃CSK₄; $n = 3$, Student's paired *t*-test $*p < 0.05$.

affect binding. To further confirm the association, MIC60 was pulled down, and an immunoblot for ataxin-3 performed (Figure 2D). Here, ataxin-3 appeared at two molecular weights, suggesting that either two separate isoforms bind to MIC60,

or it is post-translationally modified. Finally, super-resolution assessment using stimulated emission depletion (STED) microscopy confirmed that ataxin-3 was situated in close proximity to MIC60 (Figure 2E).

MIC60 is the largest protein in the mitochondrial contact site (MICOS) complex, which is embedded in the mitochondrial inner membrane and acts as a key regulator of cristae junction formation and assembly of respiratory chain complexes which are required for oxidative phosphorylation (31). Additional specific roles for MIC60 include the import of proteins (32, 33) and regulation of mitochondrial DNA (mtDNA) transcription (34, 35). Consequently, we examined the effect of ataxin-3 knockdown in moDCs on expression of mtDNA genes that encode components of the oxphos machinery. moDCs from healthy human donors were found to express either a single or double isoform of ataxin-3 with approximately equal frequency, but all detectable isoforms could be efficiently knocked down (Figure 2F). Ataxin-3 depletion led to a 2-fold upregulation of NADH-ubiquinone oxidoreductase 1 (*MT-ND1*), with a statistically significant upregulation observed for mRNA expression of two other genes from Complex I, *MT-ND3* and *MT-ND4L* (Figure 2G). In comparison, genes encoding components of Complex III, IV and V were broadly unaffected. It is noteworthy that mtDNA transcription is tightly regulated due to its close links to oxphos, and thus 1.5- to 2-fold changes in mRNA expression level represent a potentially functionally significant alteration (36). The effect of NOD2/TLR2 stimulation was examined on *MT-ND1*, the most significantly affected gene. Stimulation led to a significant upregulation in mRNA expression in both the control and ataxin-3 depleted cells, but there was significantly greater ND1 in the ataxin-3 depleted cells following stimulation (Figure 2H). Finally, to understand if these effects on Complex I genes correlate with modulation of cytokine responses, we have assessed the expression of *IL8*, *IL1 β* , *TNF*, *IL12B*, and *IL23A* in response to TLR/NOD2 signaling in human moDCs and found that ataxin-3 depletion using siRNA did not affect the levels of these cytokines (data not shown).

These results indicate a novel association between ataxin-3 and MIC60, a component of the MICOS complex involved in the regulation of mtDNA. We demonstrated that ataxin-3 regulates mtDNA by downregulating the expression of Complex I genes, an effect increased on NOD2/TLR2 sensing.

Ataxin-3 Is Important for Optimal Mitochondrial Respiration Following NOD2 and TLR2 Stimulation

We next investigated the functional relevance of the observed changes in the expression of Complex I genes. Using short hairpin RNAs (shRNA) targeting the ataxin-3 gene (*ATXN3*), we downregulated ataxin-3 protein expression in THP-1 cells (Figure 3A). We next performed a real time analysis of oxidative phosphorylation to address the function of ataxin-3. We found that ataxin-3 depletion led to a significant reduction in all the key parameters of mitochondrial respiration assessed (Figures 3B–F).

We next determined whether NOD2/TLR2-mediated ataxin-3 phosphorylation stimulation affects mitochondrial respiration. Prolonged triggering of these PRRs led to an expected metabolic shift (37) with downregulation of oxidative phosphorylation. In the ataxin-3 depleted cells the level of oxphos remained

significantly lower than in the control cells following stimulation (Figures 3G–J). Importantly, no significant difference in mtDNA copy number was found between the control and ataxin-3 depleted THP-1 cell line (Supplementary Figure 1), suggesting that there are no differences in mitochondrial mass or turnover through mitophagy to explain the observed changes.

Taken together, this data shows that in innate immune cells, ataxin-3 is required for optimal mitochondrial respiration and this effect is enhanced following its phosphorylation on NOD2/TLR2 stimulation.

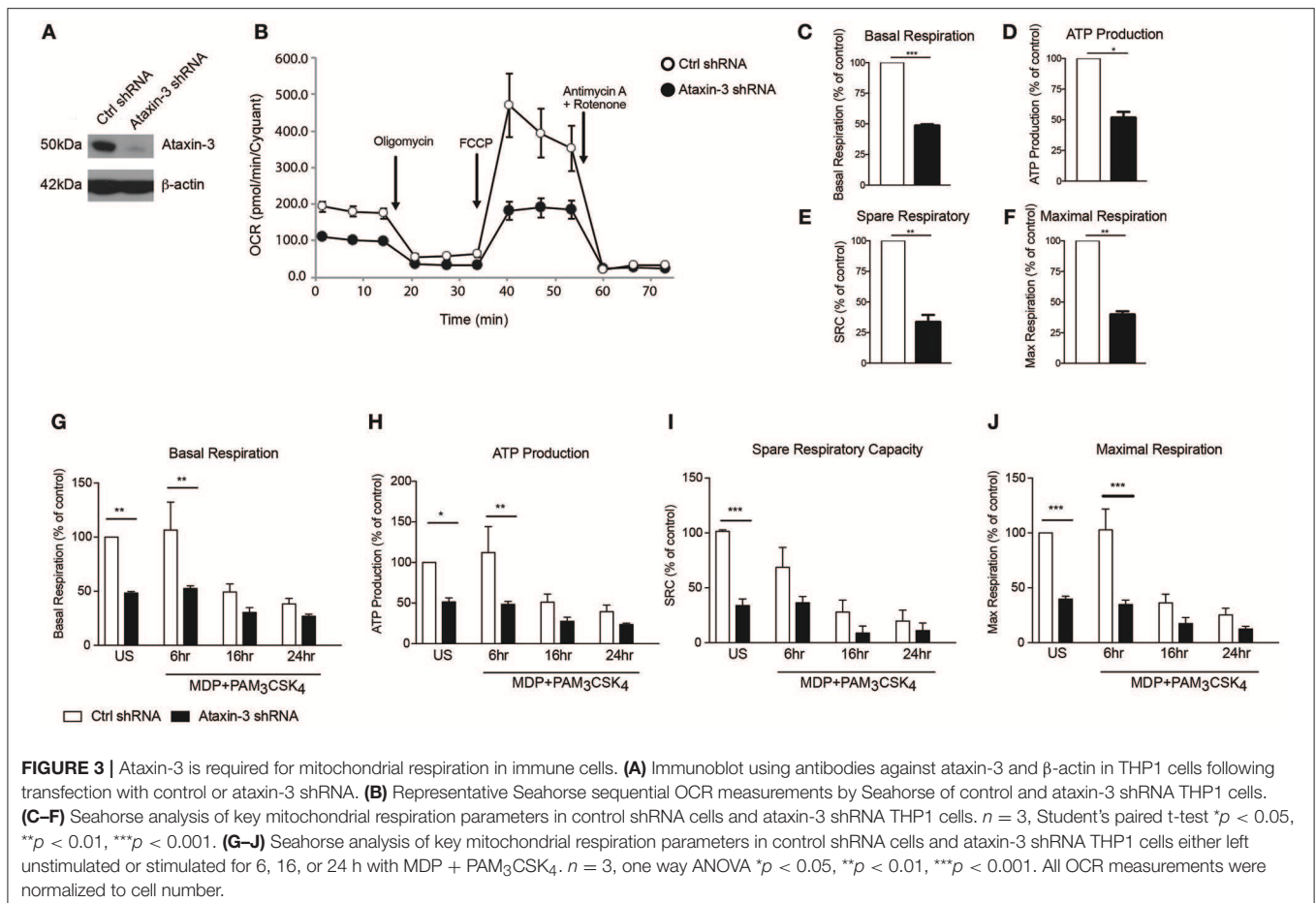
Ataxin-3 Is Required for Mitochondrial ROS Production, and Is Necessary for Optimal Bacterial Killing

A key function of mitochondrial respiration in immune cells is the generation of mROS. This results from leakage of electrons, predominantly from Complex I and to a lesser extent from Complex III, which partially reduce oxygen to form superoxide (38). The effect of ataxin-3 depletion on mROS and total cellular ROS was therefore examined. Ataxin-3 depletion led to a significant reduction in mROS (Figure 4A). As expected, there was a corresponding decrease in total cellular ROS, to which mROS makes a significant contribution (Figure 4B). The ability of immune cells to upregulate mROS production on pathogen challenge is crucial to the immune response (39); importantly, ataxin-3 depleted cells also produced less mROS on NOD2/TLR2 stimulation (Figure 4C). mROS forms an important component of antibacterial responses, and is important for bacterial killing (39). To test the functional significance of the observed impairment of mitochondrial oxphos and mROS generation on NOD2/TLR2 triggering, we assessed the response of ataxin-3 depleted macrophages to *Salmonella* Typhimurium, a Gram-negative intracellular bacterium that is sensitive to ROS-dependent killing (39, 40). A gentamicin survival assay was undertaken. While bacterial invasion was unchanged, as evidenced by similar bacterial counts at 1 h post-infection, there was subsequently significantly greater bacterial survival in the ataxin-3 depleted cells that was maximal at 6 h (Figure 4D). There were no significant differences in cell viability between the two groups at any of the infection time points (Supplementary Figure 2), excluding differences in cell survival as a contributing factor in the bacterial killing deficit.

Taken together, this data shows that in macrophages ataxin-3 is required for mROS generation and this contributes to effective intracellular bacterial killing.

An Unbiased Ubiquitome Screen Reveals Novel DUB Targets of Ataxin-3 Following NOD2 and TLR2 Activation

To further define the role of ataxin-3 in NOD2/TLR2 signaling, we sought to define downstream DUB targets. Classically the ubiquitinated proteome, also termed the ubiquitome, was first enriched using His₆-tagged ubiquitinated conjugates under denaturing conditions. However, concerns exist over the impact of overexpressed modified His₆, which competes with

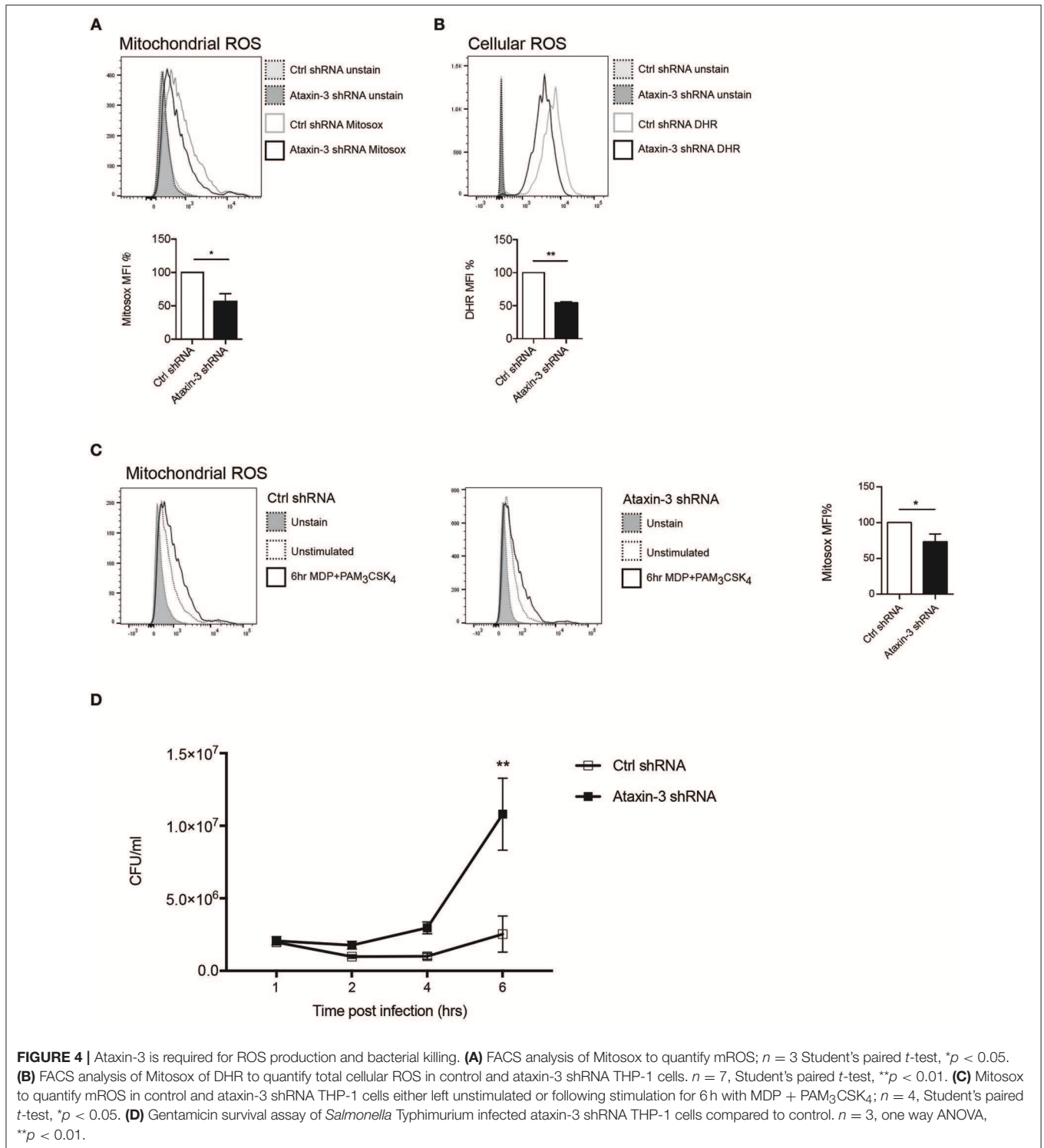


endogenous ubiquitin, on the ubiquitome (41). An alternative method of enrichment, using high affinity ubiquitin traps has therefore been developed. These tandem ubiquitin binding entities (TUBEs) specifically recognize, bind to, and stabilize polyubiquitinated proteins, protecting them from degradation by DUBs or the proteasome. The enriched ubiquitinated proteins can then be analyzed by MS (41–43). The ability of TUBEs to preferentially recognize either K48 or K63 linked polyubiquitin provides a further advantage. Consequently, the use of a K63-TUBEs1 system which shows a 10-fold higher affinity for K63 linked chains, allows the selective enrichment of the K63 linked ubiquitome. This provides a specific means of purifying the K63 chains favored by ataxin-3 (44), and thus was employed as a strategy for defining novel DUB targets of ataxin-3 in immune cells.

The TUBEs2 system was used to enrich ubiquitinated proteins in ataxin-3 depleted and control THP-1 cells, either left unstimulated or stimulated for 1 h with MDP + PAM₃CSK₄. Samples from three biological replicates were then subjected to mass spectrometry analysis (Figure 5A). As a quality control prior to MS analysis, immunoblotting with an antibody against K63-linkage specific polyubiquitin demonstrated a marked increase in the levels of K63 ubiquitinated proteins in the ataxin-3

depleted cells, most notably at higher molecular weights, with NOD2/TLR2 stimulation leading to a separate shift in staining pattern (Figure 5B).

Mass spectrometry analysis identified 291 proteins as changing significantly between any condition when averaged across the three biological replicates. As ataxin-3 acts as a DUB, ataxin-3 depletion would classically lead to an accumulation of ubiquitinated targets and thus particular attention was paid to those proteins that showed an increase in abundance in the ataxin-3 depleted samples (Supplementary Table 2). However, as deubiquitination can also regulate protein stability, it is likely that a number of the proteins found to decrease in abundance on ataxin-3 depletion are also direct DUB targets of ataxin-3. Most notably, the immunometabolic regulator HIF1 α (45) was found to be more abundant in the ataxin-3 depleted cells, suggesting that ataxin-3 may deubiquitinate HIF1 α (Figure 5C). To specifically interrogate the importance of NOD2/TLR2 phosphorylation of ataxin-3 on DUB activity, the abundance of proteins in the ataxin-3 depleted cells was compared to the control cells following stimulation with MDP + PAM₃CSK₄ (Supplementary Table 3). Strikingly, a cluster of proteins related to metabolism were noted in the ataxin-3 depleted cells (marked in red on Figure 5D).



Ataxin-3 Deubiquitinates HIF, PLD3, and LAMTOR1 Upon NOD2 and TLR2 Activation

A number of the proteins from the mass spectrometry analysis were selected for further validation. HIF1 α was of particular interest given its central role in immunometabolism. Although

classically described as part of the family of hypoxia-inducible factor regulators, mediating the cellular response to hypoxia (46), more recent work has demonstrated a broader role in regulation of the immune system. It is important for both the survival and function of cells of the innate immune system,

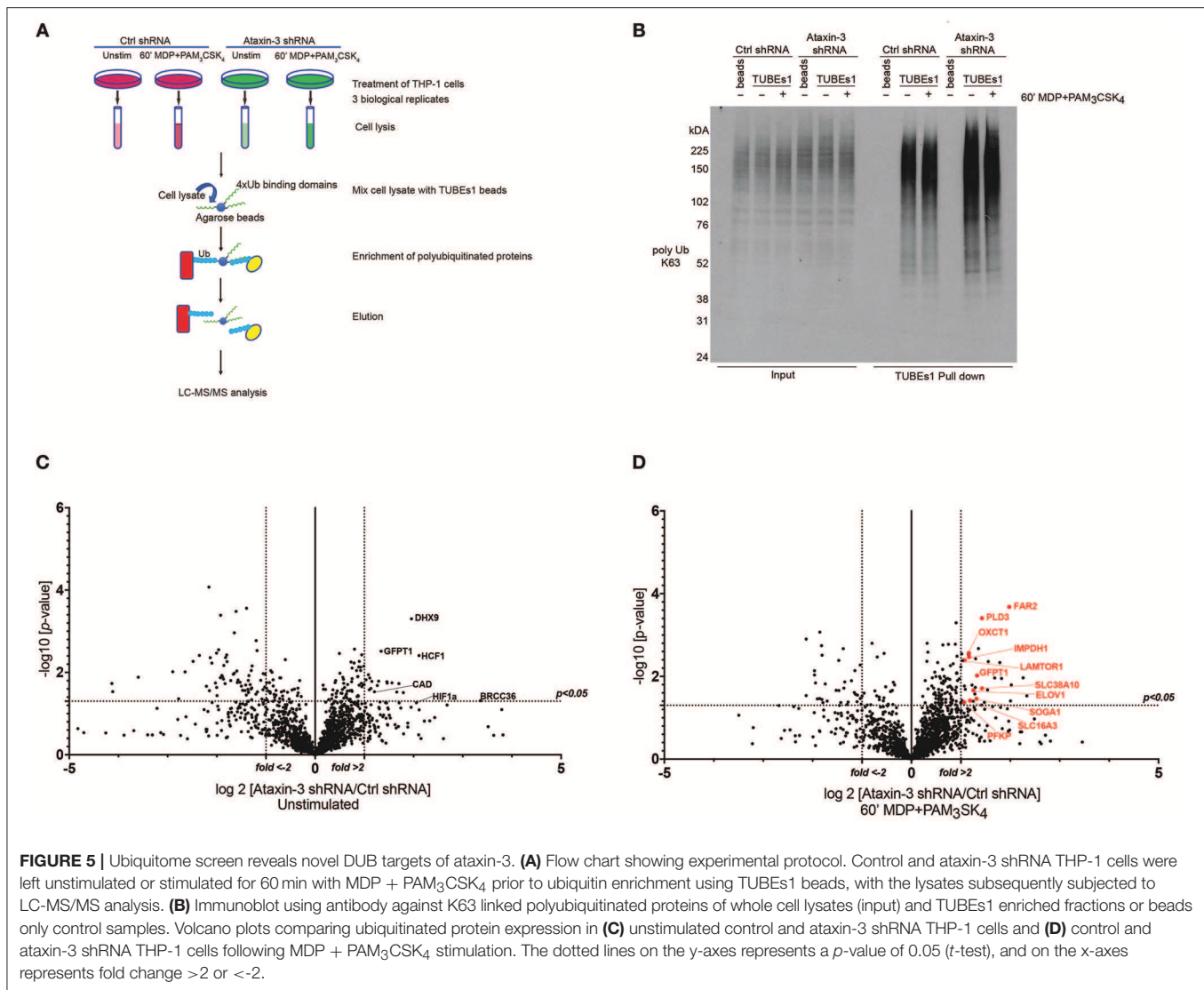


FIGURE 5 | Ubiquitome screen reveals novel DUB targets of ataxin-3. **(A)** Flow chart showing experimental protocol. Control and ataxin-3 shRNA THP-1 cells were left unstimulated or stimulated for 60 min with MDP + PAM₃CSK₄ prior to ubiquitin enrichment using TUBE1 beads, with the lysates subsequently subjected to LC-MS/MS analysis. **(B)** Immunoblot using antibody against K63 linked polyubiquitinated proteins of whole cell lysates (input) and TUBE1 enriched fractions or beads only control samples. Volcano plots comparing ubiquitinated protein expression in **(C)** unstimulated control and ataxin-3 shRNA THP-1 cells and **(D)** control and ataxin-3 shRNA THP-1 cells following MDP + PAM₃CSK₄ stimulation. The dotted lines on the y-axis represents a *p*-value of 0.05 (*t*-test), and on the x-axis represents fold change >2 or <-2.

through regulation of metabolic activation (47–49). HIF1 α was validated as a DUB target of ataxin-3 through immunoblot, with a significant increase in ubiquitinated HIF1 α in the ataxin-3 depleted cells (**Figure 6A**). HIF1 α was detected in the whole cell lysates of both control and ataxin-3 depleted cells in normoxia, as the proteasome inhibitor MG132 which reduces the degradation of all ubiquitinated proteins was added to the cell suspension 30 min before the end of all TUBE1 experiments.

Phospholipase D3 (PLD3) was also intriguing as it has recently been shown to regulate inflammatory cytokine responses in response to TLR9 signaling by acting as an endonuclease (50). In humans, mutations confer an increased risk for the neurodegenerative diseases Alzheimer's (51) and spinocerebellar ataxia (52), with increasing evidence of the role of innate immune dysfunction in neurodegeneration (53). Importantly, polyglutamine repeat mutations in ataxin-3 are themselves associated with the spinocerebellar ataxia Machado-Joseph disease (18). Regulator complex protein LAMTOR1 forms

part of the Regulator complex essential for amino acid sensing and activation of mTORC1 (54), but has also been linked to independent roles in lysosomal maturation (55) and M2 macrophage differentiation (56). PLD3 and LAMTOR1 were both validated by immunoblot (**Figures 6B,C**). Ataxin-3 depletion led to accumulation of ubiquitinated forms of both PLD3 and LAMTOR1. Notably, NOD2/TLR2 stimulation increased LAMTOR1 ubiquitination in the control cells, but there was markedly more LAMTOR1 ubiquitination in the stimulated ataxin-3 depleted cells (**Figure 6C**). This suggests that ataxin-3 modulates the ubiquitination of LAMTOR1 induced by NOD2/TLR2 stimulation.

To further study the interaction between LAMTOR1 and ataxin-3, an overexpression system was employed in the human cell line HEK293. HA-ataxin-3 and GFP-LAMTOR1 was overexpressed, together with a GFP-control and then IP of HA-ataxin-3 performed using an antibody against the HA tag. Ataxin-3 was found to bind directly to LAMTOR1 (**Figure 6D**). Next,

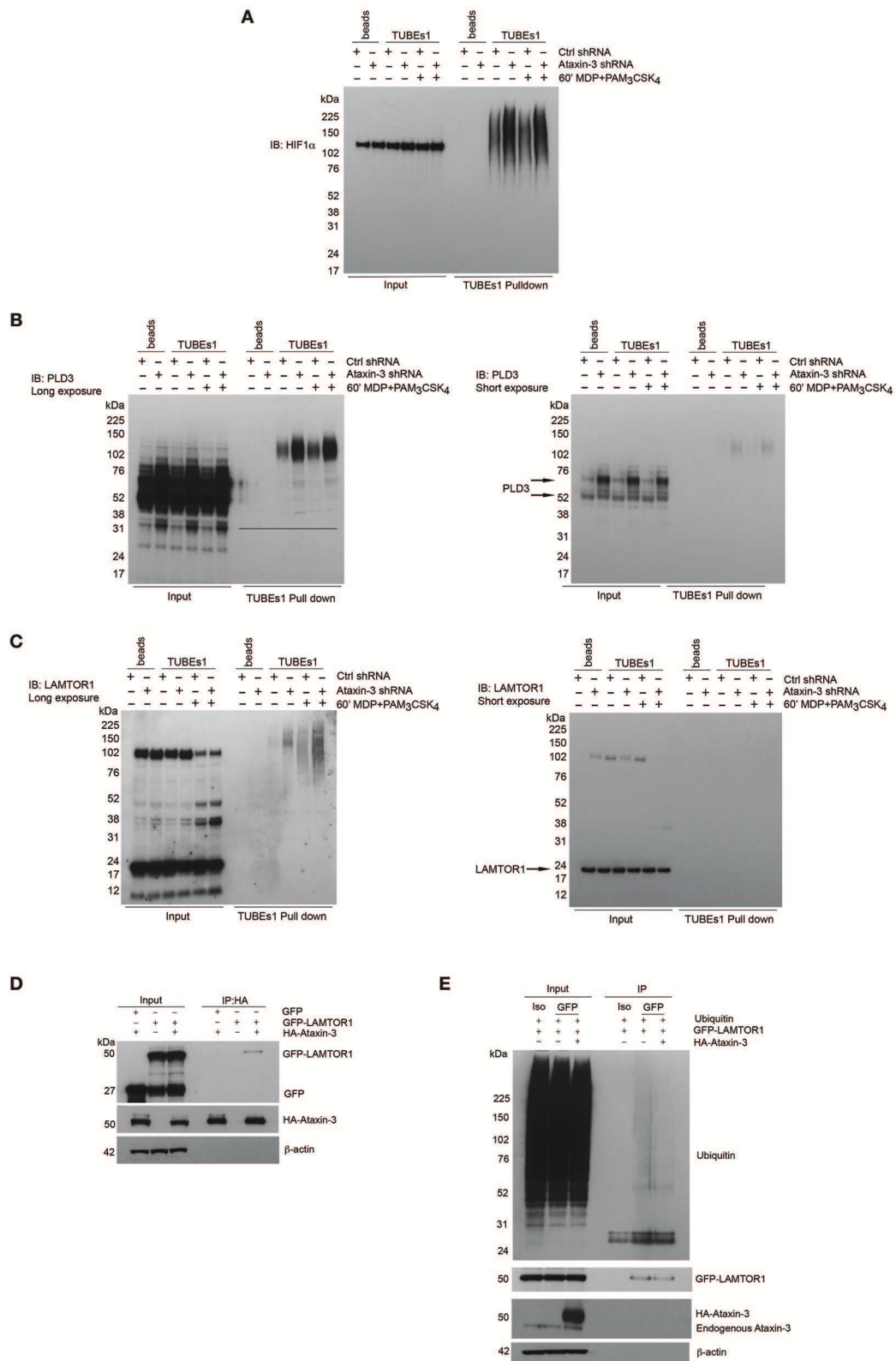


FIGURE 6 | Validation of novel DUB targets of ataxin-3. **(A)** Immunoblot using antibody against HIF1a in whole cell lysate (input) and TUBEs1 enriched fractions from control and ataxin-3 shRNA THP-1 cells left unstimulated or stimulated for 60 min with MDP + PAM₃CSK₄. Immunoblot using antibodies against **(B)** PLD3 and *(Continued)*

FIGURE 6 | (C) LAMTOR1 in whole cell lysates (input) and TUBEs1 enriched fractions from control shRNA and ataxin-3 shRNA THP-1 cells left unstimulated or stimulated for 60 min with MDP + PAM₃CSK₄. **(D)** Immunoblot using antibodies against GFP, HA, and β -actin in input and HA-immunoprecipitated lysates, in HEK293 cells where GFP and/or GFP-LAMTOR1 and/or HA-ataxin-3 were overexpressed. **(E)** Immunoblot using antibodies against ubiquitin, GFP, ataxin-3, and β -actin in input and isotype control (iso) or GFP immunoprecipitated lysates where ubiquitin and GFP-LAMTOR1 were overexpressed with or without HA-ataxin-3. All immunoblots are representative of at least two independent experiments.

the finding that LAMTOR1 is a direct DUB target of ataxin-3 was confirmed. Ubiquitin, GFP-LAMTOR1 and HA-ataxin-3 were overexpressed in HEK293 cells and IP of GFP-LAMTOR1 performed using an antibody against the GFP tag. The level of ubiquitinated GFP-LAMTOR1 was found to be significantly less in cells where HA-ataxin-3 was co-expressed (**Figure 6E**).

Taken together, these results show that ataxin-3 modulates the ubiquitination of previously unidentified targets related to metabolism. This effect is enhanced on following phosphorylation of ataxin-3 on NOD2/TLR2 triggering.

DISCUSSION

In this study we demonstrate that NOD2 and TLR2 phosphorylates the deubiquitinase ataxin-3 at serine 265 through a signaling cascade involving RIPK2 and TBK1. Immunoprecipitation and MS analysis of interacting partners established an association with a core component of the mitochondrial MICOS complex MIC60. Ataxin-3 was subsequently shown to be necessary for optimal mitochondrial respiration and mitochondrial ROS generation in macrophages, an effect enhanced by its phosphorylation on NOD2/TLR2 triggering. In line with this, we found that ataxin-3 is required for optimal intracellular bacterial killing of *Salmonella* Typhimurium. Finally, we dissected the specific DUB role of ataxin-3 in an immune context through an unbiased MS screen of the ubiquitome. A preponderance of metabolism related proteins were discovered including HIF1 α , phospholipase D3 and LAMTOR1, underlining a central role of ataxin-3 in immunometabolism.

Deubiquitinating enzymes (DUBs) represent specialized proteases which modify ubiquitin chains by cleaving the isopeptide bonds linking the ubiquitin C-terminus to a lysine side chain on the target protein. Modification of ubiquitination may alter cellular responses through regulation of target protein stability, or mediate signal transduction through non-degradative pathways including mediation of protein-protein interactions (57). Ataxin-3 is a small protein, consisting of 364 amino acids, that is ubiquitously expressed (58). At the N-terminus there is a catalytic Josephin domain, which acts as a protease that hydrolyses ubiquitin linkages and allows ataxin-3 to function as a DUB (59). A flexible C-terminal tail contains either two or three ubiquitin-interacting motifs (UIMs), according to the isoform (60). The UIMs mediate selective binding to ubiquitin chains, determining the type of chain that can be cleaved by the Josephin domain. Ataxin-3 shows a preference for cleavage of K63-Ub chains, although it is able to bind both K63 and K48 chains (44).

Ataxin-3 has been linked to neurodegenerative disease after unstable CAG repeat expansions in the ATXN3 gene were

identified as the cause of spinocerebellar ataxia Type 3 (SCA3), also known as Machado-Joseph Disease, the most common autosomal dominant ataxia (18). Importantly, the expanded polyglutamine stretch results in more complex sequelae than a simple loss of protein function, and likely leads to a toxic gain of function through altered binding properties, aggregation and subcellular localization (61). Accumulating evidence suggests that ataxin-3 performs diverse cellular roles, including DNA repair (62, 63) and transcriptional regulation (64), regulation of protein quality through endoplasmic reticulum (ER) associated degradation (65) and aggresome formation (66), and beclin-1 dependent autophagy (17). A recent study provided a first link to immune regulation, demonstrating that ataxin-3 regulates Type 1 interferon antiviral responses through interaction with histone deacetylase 3 (HDAC 3) (67). The present study is the first to link ataxin-3 to PRR signaling and demonstrate its importance in mitochondrial respiration in macrophages, following the discovery that ataxin-3 associates with the mitochondrial protein MIC60.

MIC60 forms a core part of the MICOS complex, which is embedded in the mitochondrial inner membrane. It acts as a key regulator of mitochondrial inner membrane shape and organization. This is essential for cristae junction formation and assembly of respiratory chain complexes which are required for oxidative phosphorylation (31). MIC60 also appears to act independently of the MICOS complex, and has recently been implicated in regulation of mtDNA transcription (35). The mitochondrial genome encodes just 13 proteins, all essential components of oxfos complexes I, III and IV. In keeping with this known function of MIC60, we found that depletion of ataxin-3 led to specific upregulation of mtDNA transcripts encoding proteins required for Complex I, and this was further upregulated by NOD2/TLR2 stimulation. In addition, specific interrogation of mitochondrial oxidative phosphorylation through use of the Seahorse platform demonstrated that ataxin-3 depletion led to a particularly striking impairment in maximal respiration and spare respiratory capacity (SRC). SRC represents the extra mitochondrial capacity available within a cell to produce energy under conditions of increased work or stress and is important for cellular function and survival (68–70). Macrophages increase their SRC in response to bacterial infection to drive anti-microbial responses, and this is coordinated in part by modulation of the ETC Complexes I and II (71). In M2 macrophages, SRC is critical for their activation and prolonged survival, and clearance of the parasitic helminth (72). We found that ataxin-3 depletion impaired mROS production at both baseline and in response to NOD2/TLR2 stimulation, demonstrating the functional relevance of the observed mitochondrial respiratory impairment. Finally, we demonstrated the importance of ataxin-3 in intracellular killing

of the pathogen *Salmonella* Typhimurium, with PRR mediated mROS generation well-established as critical for destruction of this bacterium (39).

Fewer than 100 DUBs are thought to be responsible for regulating the ubiquitination of tens of thousands of proteins in a tightly regulated and sophisticated manner (57, 73). Hence defining the wide-ranging DUB targets of ataxin-3 is essential to decipher its functions. Ubiquitin signaling represents an indispensable mechanism of regulating both the innate and adaptive immune response, and is central to the NOD2 cascade (74). For the first time, this study undertook an unbiased screen of the ubiquitome in ataxin-3 depleted cells. Notably, a significant number of metabolism related proteins were found, further reinforcing the potential importance of ataxin-3 in cellular immunometabolism.

The discovery that HIF1 α is a DUB target of ataxin-3 in macrophages is noteworthy, given the emergency of HIF1 α as a key immunometabolic regulator. Work in a conditional HIF1 α knockout mouse, targeting the myeloid lineage, demonstrated the critical requirement of HIF1 α for inflammatory responses (75). This correlated with defects in glycolysis and metabolic activation, which is tightly regulated by HIF1 α . The endolysosomal protein PLD3 was also validated as a further novel DUB target of ataxin-3. Although PLD3 contains two phosphodiesterase domains, and hence is classed as a member of the phospholipase diesterase (PLD) family which act to hydrolyse phospholipids, the phospholipase activity of PLD3 has not been definitively established. The importance of PLDS in immunity was recently demonstrated, with the discovery that it acts as a single-stranded acid exonuclease that breaks down ligands for the PRR TLR9, hence regulating TLR9 mediated inflammatory responses in collaboration with PLD4 (50).

The discovery in the present study that NOD2/TLR2 triggering leads to deubiquitination of LAMTOR1 by ataxin-3 is of particular interest. LAMTOR1, also known as p18, is a late endosome/lysosome membrane adapter protein that localizes to the lipid rafts of these organelles (76, 77). LAMTOR1 plays an essential role in the activation of the mTORC kinase complex in response to amino acid levels (54). Through a mechanism involving the lysosomal v-ATPase in the presence of amino acid sufficiency, LAMTOR1 forms a scaffold at the lysosomal membrane with LAMTOR2,3,4 and 5 (the pentameric Ragulator complex) for the Rag GTPase complex (RagAB/CD) (54, 78, 79). This leads to the recruitment and activation of mTORC1 which inhibits autophagy. The lysosomal v-ATPase-Ragulator complex also activates another critical metabolic sensor, AMP-activated protein kinase (AMPK), which responds to falling energy levels by driving cellular catabolism programmes and downregulating anabolic pathways (80). Thus, this complex is able to respond to both energy/nutrient sufficiency and deficiency. Strikingly, of all cells, macrophages express the highest levels of the five Ragulator components, suggesting their importance in the immune response (81). Indeed, LAMTOR1 was recently found to be essential for the polarization of M2 macrophages both *in vitro* and *in vivo* in a knockout mouse model, by coupling metabolism to immunity (56).

The physiological importance of NOD2 and TLR2 in both the innate and adaptive immune response is well-established. The interplay between NOD2 and TLR2 has been well-characterized given the fact that they both respond to adjacent components of PGN found in the bacterial cell walls. The NOD2 signaling pathway amplifies TLR2 activation and both receptors synergize in the induction of cytokine production. *NOD2* variants confer the greatest single genetic risk factor for Crohn's disease (2, 3), yet significant gaps remain in our knowledge of how this receptor exerts its effects (82). Notably, despite the recent explosion of interest in the field of immunometabolism, almost nothing is known about how the synergistic effects of NOD2 and TLR2 signaling might intersect with metabolic pathways to modulate the immune response. Here, we defined the molecular and functional basis by which NOD2/TLR2 sensing links to ataxin-3 and, consequently, other immunometabolic factors. Future studies are required to provide novel prospects for modulating these pathways as new therapeutic strategies for inflammatory disorders.

MATERIALS AND METHODS

Cells

Human monocytes were purified from healthy donor peripheral blood mononuclear cells (PBMCs) by positive immunoselection with anti-CD14-conjugated MACS beads (Miltenyi Biotec). moDCs were obtained by culturing monocytes for 5 days with IL-4 and GM-CSF (PeproTech). Immature moDCs were harvested on day 5 of culture. The human THP-1 cell line was purchased from ATCC. Prior to use, THP-1 were differentiated by treatment with 25 ng/ml phorbol 12-myristate 13-acetate (PMA) (Sigma) for 16 h.

Reagents and Antibodies

The following stains were used: MitoSox Red M36008 (Invitrogen) and DHR 123 D23806 (Invitrogen). Antibodies include mouse anti-human ataxin-3 65042 1H9-2 (BioLegend), mouse anti-human MIC60 ab110329 (Abcam), mouse anti-human MIC60 ab137057 (Abcam), rabbit anti-human TBK1 #3504 D1B4 (Cell Signaling), rabbit anti-human RIPK2 #4142 D10B11 (Cell Signaling), rabbit anti-human p38 #9212 (Cell Signaling), rabbit anti-human LAMTOR1 #8975 D11H6 (Cell Signaling), rabbit anti-human PLD3 HPA012800 (Sigma), rabbit anti-human HA #3724 C29F4 (Cell Signaling). The secondary antibodies included: anti-rabbit HRP conjugate #7074 (Cell Signaling), anti-mouse HRP conjugate #7076 (Cell Signaling), goat anti-rabbit Alexa fluor 488 A-11034 (Invitrogen), goat anti-rabbit Alexa fluor 488 A-11029 (Invitrogen), goat anti-mouse Alexa fluor 568 A-11036 (Invitrogen), goat anti-rabbit Alexa fluor 568 A-11004 (Invitrogen). Beta actin HRP conjugate #5125 (Cell Signaling). For qPCR, the following Taqman primers were used (all ThermoFisher): NOD2 (Hs01550753_m1), RPLP0 (Hs99999902_m1), MT-ND1 Hs02596873_s1, MT-ND2, Hs02596874_g1, MT-ND3 Hs02596875_s1, MT-ND4L Hs02596877_g1, MT-CYB Hs02596867_s1, MT-CO1 Hs02596864_g1, ATP6, Hs02596862_g1. For overexpression

experiments, GFP-LAMTOR1 and HA-ataxin-3 were obtained from the University of Dundee.

Cell Stimulation

moDCs and THP-1 cells were left unstimulated or stimulated with 10 $\mu\text{g/ml}$ MDP or 1 $\mu\text{g/ml}$ PAM₃CSK₄ (Invivogen) or both at the indicated time points. In some experiments, other PRR ligands were used including LPS 100 ng/ml, and R848 1 $\mu\text{g/ml}$ (Invivogen) or cells were treated with the small molecule inhibitor Ponatinib (50 nM) for 1 h.

Phosphoprotein Purification

Cells were harvested on ice and washed once with ice cold modified Hanks Buffered Saline (HBS) (20 mM HEPES pH 7.4, 150 mM NaCl in ddH₂O). Cell pellets were lysed in Qiagen "Phosphoprotein lysis buffer" containing 0.25% (v/v) CHAPS with 1% (v/v) phosphatase inhibitor cocktail 3 (Sigma), protease inhibitor tablet (Qiagen) and the nuclease 0.0002% (v/v) Benzonase (Qiagen) at 4°C for 40 min, with vortexing every 10 min. Cell debris was removed by centrifugation of the lysate at 13,300 rpm for 30 min at 4°C. The clarified supernatant was then transferred to fresh pre-cooled tubes and protein concentration determined by BCA assay. The samples were then diluted in Qiagen "wash buffer" containing 0.25% (v/v) CHAPS to a concentration of 0.1 mg/ml. Aliquots of whole cell lysate and diluted whole cell lysate were kept for subsequent immunoblot. The phosphoenrichment columns were washed with 6 ml "wash buffer," before the diluted samples were loaded onto the columns. Following two further washes of the columns with 6 ml "wash buffer," the phosphoenriched fraction was eluted from the columns using Qiagen "elution buffer" containing 0.25% (v/v) CHAPS. Following concentration of the eluted fraction to a volume of 200–300 μl using 9k molecular weight cut-off concentrator columns (Thermo Fisher) with centrifugation 13,000 rpm 30 min, protein concentration was measured by BCA. For mass spectrometry (MS) experiments, phosphoenriched lysates were stored at –80°C. Otherwise, whole cell lysate, diluted whole cell lysate and phosphoenriched lysates were processed for SDS-PAGE with NuPage LDS Sample buffer (Life Technologies) and 100 mM dithiothreitol (Sigma), followed by heating at 70°C for 5 min. Samples were then frozen at –80°C until immunoblotting was performed.

Immunoprecipitation

Samples were washed twice in ice cold HBS and then lysed in 1,000 μl lysis buffer for 30 min at 4°C with end over end mixing [Cell Signaling Lysis Buffer 20 mM Tris-HCL pH7.5, 1 mM Na₂EDTA, 1 mM EGTA, 1% Triton, 2.5 mM sodium pyrophosphate, 1 mM beta-glycerophosphate, 1 mM Na₃O₄, 1 $\mu\text{g/ml}$ leupeptin supplemented with 1% (v/v) HALT protease inhibitor cocktail (Thermo Fisher) and 1% (v/v) Phosphatase inhibitor cocktail 2 and 3 (Sigma) and 1 mM PMSF (Cell Signaling)]. Lysates were clarified by centrifugation at 14,000 g for 15 min at 4°C, and the supernatant transferred to fresh Eppendorfs. Protein concentrations were calculated by BCA.

Fifty μl of input lysate was heated with LDS/DTT and stored at –80°C for later immunoblot. Next, concentrations were adjusted to 1 mg/ml and 7.5 mg of protein was taken forward for IP for each condition. The appropriate antibody or isotype control antibody was added to the lysates followed by incubation with gentle end over end mixing at 4°C overnight.

The next morning, Protein G Dynabeads (Thermo Fisher) were washed once in lysis buffer, using a DynaMag2 magnet (Invitrogen) to separate the beads from solution, and 5 μl of beads per 1 μg of antibody was added to each sample. Samples were incubated with the beads with gentle end over end mixing for 2 h at 4°C. Following this, the supernatant was removed using a magnet to separate the beads, with 50 μl of the supernatant heated with LDS/DTT and stored at –80°C later immunoblot. The beads were washed 4 times in total with lysis buffer containing all protease and phosphatase inhibitors, with gentle end over end mixing for 5 min at 4°C for each wash. Elution of the beads was then performed by incubating the beads with pH 2.8 elution buffer (Pierce) with gentle end over end mixing for 30 min at 4°C. The eluate was collected and neutralized immediately with 1/10 volume of 1 M Tris-HCL pH 9. Elution and neutralization was performed a further two times to ensure complete elution. The eluate was stored at –80°C until used for downstream processing.

Tandem Ubiquitin Binding Entities (TUBEs) Ubiquitin Immunoprecipitation

Typically 2.5×10^7 THP-1 cells were used per condition. Thirty min before the end of the experimental conditions, samples were incubated with 10 μM MG132 (Sigma) for 30 min at 37°C before harvesting, washing once in ice cold PBS and lysing in 1 ml Ub-IP lysis buffer (50 mM Tris-HCL (pH 8.0), 150 mM NaCl, 5 mM EDTA, 1% NP-40, 0.5% Deoxycholate, 0.1% SDS, protease inhibitor cocktail (Roche), 1% (v/v) phosphatase inhibitor cocktail 3 (Sigma), 20 μM MG132, 50 μM PR619 and 100 mM N-ethylmaleimide (Sigma)). Cells were lysed for 30 min at 4°C with gentle end over end mixing. The lysate was clarified by centrifugation at 13,000 rpm for 20 min at 4°C, and the supernatant transferred to fresh Eppendorfs. Protein concentration was calculated by the Bradford assay and protein concentrations normalized to 2 mg/ml. Typically 2 mg of protein was taken forward for TUBEs IP. Fifty μl of input fraction was heated with LDS/DTT and stored at –80°C for later immunoblot. Samples were incubated with 40 μl TUBE1 agarose beads (LifeSensors), or control agarose beads (LifeSensors) for 4 h at 4°C with gentle end over end mixing. The beads were then centrifuged at 3,000 g for 3 min and washed with lysis buffer containing all inhibitors three times (each wash was performed for 5 min at 4°C with gentle end over end mixing), followed by two final washes with lysis buffer without SDS and Deoxycholate. Elution was then performed with 50 μl of pH 2.8 elution buffer (Pierce) for 30 min with gentle end over end mixing at 4°C, followed by immediate neutralization with 1/10 volume 1 M Tris-HCL pH 9. Elution and neutralization was performed three times in total. Samples prepared for later MS analysis were frozen at –80°C until further processing (100 of 150 μl total eluate). The

remaining 50 μ l, and all eluate from other experiments were heated with $2 \times$ LDS/DTT at 70°C for 10 min and stored at -80°C until immunoblot.

Liquid Chromatography Tandem Mass Spectrometry (LC-MS/MS)

100 μ l of lysate was adjusted to 175 μ l with ddH₂O. All samples were then successively reduced and alkylated for 30 min with 5 mM dithiothreitol and 20 mM iodoacetamide, respectively. The proteins were then precipitated using chloroform-methanol precipitation and the pellet were solubilized in 6 M urea, 0.1 M Tris pH 7.8. The sample were diluted to 1 M Urea. The digestion was performed overnight at 37°C by adding 500 ng of trypsin. The peptides were desalted using a C18 cartridge (Waters). Briefly, the samples were conditioned with buffer A (1% (v/v) acetonitrile, 0.1% (v/v) trifluoroacetic acid (TFA) in water) prior to equilibration with buffer B (65% (v/v) acetonitrile, 0.1% (v/v) TFA in water). The acidified peptides were loaded onto the column, washed with buffer A and eluted with buffer B. The solution containing the peptides was dried with a speedvac and solubilised in 1% (v/v) acetonitrile, 0.1% (v/v) TFA in water for mass spectrometry analysis.

Peptides were analyzed with nano ultra-high performance liquid chromatography tandem mass spectrometry (nano-UPLC-MS/MS) using a Dionex Ultimate 3000 nanoUPLC, coupled to an Orbitrap Fusion Lumos mass spectrometer (Thermo Scientific). MS analysis was performed essentially as described previously (83). In brief, the data were acquired with a resolution of 120,000 full-width half maximum at mass/charge 200 with EASY-IC using the reagent ion source (202 m/z) for internal calibration enabled, Top speed precursor ion selection, Dynamic Exclusion of 60s and fragmentation performed in Collision Induced dissociation (CID) mode with Collision Energy of 35.

Analysis of Mass Spectrometry Data Label-Free Quantitative Analysis

The raw MS data was analyzed using Progenesis QI (Waters) and searched using Mascot 2.5 (Matrix Science). The search settings were as follows: trypsin with 1 miscleavage allowed, oxidation (M) and Deamidation (N, Q) were set as variable modifications and carbamidomethylation (C) as fixed modification. The data was searched against human protein sequences using the UPR_homoSapiens_20141015 (85,889 sequences; 33,866,397 residues) allowing a peptide mass tolerance of 10 ppm and a fragment mass tolerance of 0.05 Da.

Peaks Search for Phosphorylation

The raw MS data was analyzed in PEAKS Studio 7.5 (Bioinformatics Solutions Inc). The settings were the following: The database used was the swissprot human database was used for the proteins identification. The enzyme used for the search was trypsin allowing a maximum of 2 miscleavages. Fixed modifications: Carbamidomethyl (C); Variable modifications: Deamidated (N), Deamidated (Q), Oxidation (M), Phospho (STY). Ten ppm mass tolerance were allowed for the precursor ions and 0.05 Da was allowed for the fragment ions.

Mascot Search for Phosphorylation

The raw MS data was searched using Mascot with following settings. Enzyme: Trypsin; Fixed modifications: Carbamidomethyl (C); Variable modifications: Deamidated (N), Deamidated (Q), Oxidation (M), Phospho (ST), Phospho (Y); Peptide mass tolerance: \pm 10 ppm (# 13C = 1); Fragment mass tolerance: \pm 0.5 Da; Max missed cleavages: 1.

shRNA Lentiviral Transduction and siRNA Transfection

Short hairpin RNA lentiviral particles were produced and transduced following the RNAi Consortium (TRC) protocols. ShRNA containing pLKO.1 vectors targeting NOD2 (SHCLND-NM_022162), ataxin-3 (SHCLND-NM_004993), TBK1 (SHCLND-NM_013254) or non-Target shRNA Control Plasmid DNA were all obtained from Sigma (MISSION shRNA Plasmid DNA). In brief, HEK293T packaging cells growing in 6 cm well plate were transfected with a mix of 1 μ g packaging vector (psPAX2), 0.4 μ g envelope vector (pMD2.G) and 1.6 μ g hairpin-pLKO.1 vector (SHC016 control or gene specific shRNA. Fugene-6 (Promega) was used as transfection reagent. Cell culture medium containing lentiviral particles (LVP) was collected 48 h later and passed through a 0.45 μ m filter (Sartorius). Virus preparations were then concentrated by centrifugation at 30,000 rpm for 90 min. Viral particles were added to cultured THP-1 cells in R10 [Roswell Park Memorial Institute medium (RPMI-1640) (Sigma) supplemented with 10% (v/v) heat-inactivated fetal calf serum (FCS) (Sigma), 2 mM (1% v/v) L-glutamine (Sigma)] together with 8 μ g/ml Polybrene (Sigma) to improve transfection efficiency. Following incubation for 3 h at 37°C, the cells were harvested, washed, and resuspended at 1×10^6 cells/ml in R10 media with antibiotics including puromycin (as selective antibiotic). After 10 days of continuous selection with puromycin, knockdown efficiency was assessed by immunoblot. Transfection of human dendritic cells was performed by electroporation of SMARTpool ONTARGETplus human ataxin-3 (ATXN3) or non-targeting siRNAs (Dharmacon). Cells were resuspended in the solution provided with the kit (Invitrogen) followed by electroporation with Neon System kit (Invitrogen) using the following parameters: 1,475 V, 20 ms, 2 pulses. After 48 h, cells were harvested for use in experiments and to check knockdown by immunoblot.

Adherent Cell Transfection

Human HEK293/NOD2 Cells were seeded 24 h prior to transfection in media without antibiotics. Transfection mixes were made, comprising Fugene (Promega) at a ratio of 3:1 to amount of DNA plasmid to be transfected, in the appropriate volume of Opti-MEM (Gibco, Thermo Fisher) (10% of volume of media in wells to be transfected). The transfection mixes were incubated at room temperature for 20 min and then added dropwise to the wells to be transfected. Cells were either cultured for a further 24 or 48 h before being used for downstream applications.

RNA Isolation

Typically $2\text{--}5 \times 10^6$ cells per condition were harvested and washed once with cold PBS. Pellets were resuspended in 350 μl RLT buffer (Qiagen) containing 1% (v/v) Mercaptoethanol (Sigma) and stored at -80°C . Samples were thawed on ice and homogenized by adding to Qiasredder columns (Qiagen) and centrifuged 2 min 13,000 rpm. RNA isolation was then performed using RNeasy kits (Qiagen) according to manufacturer's instructions. The isolated RNA was eluted by added 25 μl nuclease free water (Ambion) to the RNeasy column membrane for 5 min, followed by centrifugation into fresh Eppendorfs 8,000 g 1 min. RNA concentration and purity were obtained using a Nanodrop 1000 spectrophotometer (Thermo Fisher) and samples were stored at -20°C until further analysis.

Reverse Transcription

RNA was reverse transcribed using a high capacity RNA to cDNA kit (Applied Biosystems). Five hundred ng to 2 μg of RNA was normalized to the same concentration for each sample using nuclease free water (Ambion) in polypropylene PCR tubes (Starlab). Then an RT mix containing 2 μl $10\times$ RT buffer, 0.8 μl $25\times$ dNTP mix, 2 μl RT random primers, 1 μl multiscribe RT, 1 μl RNase inhibitor (Applied Biosystems) and 3.2 μl nuclease free water was added to each PCR tube (10 μl total RT mix) (Starlab) for a total volume of RNA sample and RT mix of 20 μl . This was reverse transcribed using a Thermo Cyclor (Applied Biosystems) with the program: 25°C 10 min, 37°C 120 min, 85°C 5 min. The cDNA was stored at -20°C .

Quantitative Real Time Polymerase Chain Reaction (qPCR)

qPCR was performed using TaqMan chemistry (Applied Biosystems). cDNA was diluted 10-fold with nuclease free water. 4.5 μl of diluted cDNA was added in triplicate for each sample to wells of a white 0.2 ml 96 well PCR microplate (Starlab). 0.5 μl of TaqMan FAM-MGB labeled primer (Applied Biosystems) and 5 μl TaqMan Universal PCR Mastermix (Applied Biosystems) was added to each well, resulting in a 10 μl total reaction mix. The plate was covered with a polyolefin optical film (Starlab) and centrifuged at 400 g for 1 min. qPCR was then performed using the Bio-Rad C1000 Thermal cycler CFX Realtime system (Bio-Rad) using the manufacturer's recommended program: 50°C 2 min, 95°C 10 min, then 40 cycles of 95°C 15 s, 60°C 1 min. Mean cycle threshold (Ct) number was calculated from the triplicate values. Relative gene expression was calculated in comparison to the housekeeping RPLP0 control. The difference in gene expression between conditions was calculated using the $2^{-\Delta\Delta\text{Ct}}$. This is derived from:

$$\Delta\text{CT} = \text{CT}(\text{targetgene}) - \text{CT}(\text{control gene})$$

$$\Delta\Delta\text{CT} = \Delta\text{CT}(\text{targetcondition}) - \text{CT}(\text{control condition}).$$

Flow Cytometry

Typically 0.5×10^6 THP-1 cells per condition were plated in 1 ml of media in 12 well plates and differentiated for 16 h with 25 ng/ml PMA (Sigma). Following differentiation, the indicated treatments were applied. Cells were then harvested with gentle

scraping and transferred to a FACS tube. The following staining protocols were then followed. Cytofluorometric evaluation was by the LSRII flow cytometer (BD Biosciences) with analysis of the data by FLOWJo.

MitoSOX Red Staining

The cells were pelleted by centrifugation and resuspended in room temperature HBSS (Thermo Fisher) to wash, then centrifuged. The cells were resuspended in 200 μl MitoSOX red solution (final concentration 5 μM MitoSOX red (Invitrogen) in HBSS) and incubated for 15 min in the 37°C cell culture incubator. Two hundred μl of HBSS was added, and the tube centrifuged. The cells were resuspended in 250 μl HBSS and cytofluorometric evaluation performed.

Dihydrorhodamine 123 (DHR) Staining

The cells were pelleted by centrifugation and resuspended in room temperature PBS to wash, then centrifuged. The cells were resuspended in 50 μl DHR solution (final concentration 2.5 $\mu\text{g}/\text{ml}$ DHR 123 (Invitrogen) in PBS) and incubated for 30 min at 37°C in a water bath. As a positive control, 50 μl of PMA (final concentration 100 ng/ml (Sigma) in PBS) was added to control samples for the final 15 min. The cells were centrifuged and then washed once with PBS, before resuspension in 200 μl FACS staining buffer. Cells were fixed with the addition of 200 μl 1% PFA and cytofluorometric evaluation performed.

Seahorse Mitochondrial Stress Assay

The Seahorse XFe96 Extracellular Flux Analyser was used to measure mitochondrial respiration and glycolysis (Seahorse Bioscience). Seahorse 96 well assay plates (Seahorse Bioscience) were coated with Cell-Tak suspension (Corning). THP-1 cells were seeded at 1.5×10^5 cells/well. Next, the optimal working concentrations of the compounds used for the mitochondrial stress test (oligomycin, FCCP and antimycin/rotenone) and the glycolysis stress test (oligomycin and 2-DG) were determined for THP-1 cells. The aim was to maximize the response to each compound with the lowest concentration possible. An XFe96 sensor cartridge (Seahorse) was hydrated overnight prior to Seahorse assays by adding 200 μl of XF calibrant solution to each well and incubating in a CO_2 free incubator at 37°C . The sensor cartridge (Seahorse) was loaded with the test drug compounds immediately prior to the assay and loaded on the Seahorse Analyser. Twenty-four h before the assay was run, cells were harvested, counted and resuspended at 1.88×10^6 cells/ml. Two ml of cell suspension was plated in 6 well plates for each condition, with or without the appropriate ligand stimulation for the required duration. On the day of the assay, 1 ml of cell suspension from each condition was harvested into 1.5 ml Eppendorf tubes. For the mito stress test, cells were resuspended in mito stress test media with or without ligand(s) (XF base media (Seahorse Bioscience) supplemented with 1 mM sodium pyruvate (Sigma), 5 mM glucose (Life Technologies) and 2% FCS (Sigma) adjusted to pH 7.4 at 37°C and sterile filtered). Eighty μl of cell suspension (1.5×10^5 cells) was then seeded in quadruplicate for each condition and the plate was centrifuged at 200 g for 1 min. Following 30 min in a CO_2 free incubator at 37°C , 95 μl of fresh mito stress test media was

added to each well, and after a further 15 min in a CO₂ free incubator the assay was run. Final concentrations of injected drugs were 1 μM oligomycin, 1 μM FCCP, 0.3 μM rotenone and 0.3 μM antimycin.

STED Immunofluorescence Microscopy

Cells were plated in 8-well detachable tissue culture chambers on a PCA slide (Sarstedt) coated with 0.01% poly-L-lysine (Sigma)—cells were at a density of 1–2 × 10⁵ cell per well in 250 μl of appropriate media. At the end of the experiment, cells were washed twice with PBS, fixed with 4% paraformaldehyde (Sigma) for 15 min and permeabilized with 0.5% (v/v) Triton X-100 (Sigma). Cells were blocked overnight at 4°C with 150 μl blocking solution per well (5% (v/v) human serum (Sigma), 5% (v/v) goat serum (Sigma), 5% (v/v) FCS (Sigma)). The following day, cells were incubated with primary antibody diluted in 140 μl blocking solution at a pre-optimized or manufacturer recommended concentration for 1 h at room temperature. Following three washes with PBS (250 μl per well, 5 min gentle shaking), cells were incubated with the species appropriate fluorescently labeled secondary antibody for 1 h at room temperature. Cells were washed three further times with PBS, and the detached slide was then mounted with Vectashield mounting media containing DAPI (Vector Laboratories). Alternatively, cells were incubated with 200 μl PBS containing 1:100 DAPI (Thermo Fisher) for 15 min at room temperature and the detached slide was mounted with Vectashield mounting media without DAPI (Vector Laboratories). A Leica SP8 STED system was used for imaging. ImageJ was used for image processing and analysis.

Bacterial Killing Assay

1 × 10⁶ THP-1 cells were seeded per condition in 1 ml R10 without antibiotics in a 24 well plate, and differentiated overnight with 25 ng/ml PMA. After 16 h, the media was changed for 500 μl fresh R10 media without antibiotics. Two h later, *Salmonella enterica* serovar Typhimurium strain LT2 (ATCC 700220) was added at a multiplicity of infection (MOI) of 20:1. Thirty min post-infection, wells were washed twice with PBS and 500 μl fresh R10 supplemented with Gentamicin 100 μg/ml was added. After a further thirty min, wells were washed once with PBS and 500 μl fresh R10 supplemented with Gentamicin 30 μg/ml was added. At the end of the designated post-infection period, the medium was removed (and stored at –80°C until later analysis by ELISA) and 500 μl of PBS with 1% (v/v) saponin was added to the wells, followed by incubation for 5 min at 37°C. Five hundred μl of PBS was added and serial dilutions plated on LB/agar plates, incubated overnight at 37°C, and colonies then counted.

REFERENCES

1. Takeuchi O, Akira S. Pattern recognition receptors and inflammation. *Cell*. (2010) 140:805–20. doi: 10.1016/j.cell.2010.01.022
2. Ogura Y, Bonen DK, Inohara N, Nicolae DL, Chen FF, Ramos R, et al. A frameshift mutation in NOD2 associated with susceptibility to Crohn's disease. *Nature*. (2001) 411:603–6. doi: 10.1038/35079114
3. Hugot JP, Chamaillard M, Zouali H, Lesage S, Cézard JP, Belaiche J. Association of NOD2 leucine-rich repeat variants with susceptibility

Alternatively, when cell viability post-infection was assessed, cells were detached by incubating with 500 μl of trypsin per well for 5 min at 37°C, then viability assessed by trypan blue staining (Invitrogen) and counting of live/dead cells.

Statistical Analysis

Prism (GraphPad) was used to determine the statistical significance. When making multiple comparisons on a data set, analysis was by one-way ANOVA with *post-hoc* Bonferroni analysis. For experiments with two sample groups (one condition, one control) and a single comparison, analysis was by paired, two-tailed Student's *t*-test. Error bars represent Standard Error of the Mean (SEM).

DATA AVAILABILITY

The MS proteomics data is available upon request from the authors.

ETHICS STATEMENT

Ethical approval for the study was obtained from National Research Ethics Service (NRES) Sheffield Research Ethics Committee (REC reference: 16/YH/0247) and from West Midlands - The Black Country Research Ethics Committee (REC reference: 09/H1204/30).

AUTHOR CONTRIBUTIONS

TC, DC, and AS designed experimental studies, interpreted the data, and wrote the manuscript. TC, DC, SS, SP, AA, SW, MdC, M-LT, RF, and BK performed experiments, acquired, and analyzed data. HP and BK provided critical reagents, helped interpret data. AS supervised and obtained funding.

FUNDING

This work was supported by the UK MRC and by a Wellcome Investigator Award to AS, an NIHR Research Professorship to AS, and a Wellcome Clinical Training fellowship to TC. TC was also supported by the NIHR Biomedical Research Center, based at Oxford University Hospitals Trust, Oxford.

SUPPLEMENTARY MATERIAL

The Supplementary Material for this article can be found online at: <https://www.frontiersin.org/articles/10.3389/fimmu.2019.01495/full#supplementary-material>

to Crohn's disease. *Nature*. (2001) 411:599–603. doi: 10.1038/35079107

4. Corridoni D, Arseneau KO, Cominelli F. Functional defects in NOD2 signaling in experimental and human Crohn disease. *Gut Microbes*. (2014) 5:340–4. doi: 10.4161/gmic.28404
5. Girardin SE, Boneca IG, Viala J, Chamaillard M, Labigne A, Thomas G, et al. Nod2 is a general sensor of peptidoglycan through muramyl dipeptide (MDP) detection. *J Biol Chem*. (2003) 278:8869–72. doi: 10.1074/jbc.C200651200

6. Philpott DJ, Sorbara MT, Robertson SJ, Croitoru K, Girardin SE. NOD proteins: regulators of inflammation in health and disease. *Nat Rev Immunol.* (2014) 14:9–23. doi: 10.1038/nri3565
7. Brain O, Owens BM, Pichulik T, Allan P, Khatamzas E, Leslie A, et al. The intracellular sensor NOD2 induces microRNA-29 expression in human dendritic cells to limit IL-23 release. *Immunity.* (2013) 39:521–36. doi: 10.1016/j.immuni.2013.08.035
8. Corridoni D, Chapman T, Ambrose T, Simmons A. Emerging mechanisms of innate immunity and their translational potential in inflammatory bowel disease. *Front Med.* (2018) 5:32. doi: 10.3389/fmed.2018.00032
9. Corridoni D, Simmons A. Innate immune receptors for cross-presentation: the expanding role of NLRs. *Mol Immunol.* (2017). doi: 10.1016/j.molimm.2017.11.028. [Epub ahead of print].
10. Cooney R, Baker J, Brain O, Danis B, Pichulik T, Allan P, et al. NOD2 stimulation induces autophagy in dendritic cells influencing bacterial handling and antigen presentation. *Nat Med.* (2010) 16:90–7. doi: 10.1038/nm.2069
11. Cao X. Self-regulation and cross-regulation of pattern-recognition receptor signalling in health and disease. *Nat Rev Immunol.* (2016) 16:35–50. doi: 10.1038/nri.2015.8
12. Netea MG, Ferwerda G, de Jong DJ, Jansen T, Jacobs L, Kramer M, et al. Nucleotide-binding oligomerization domain-2 modulates specific TLR pathways for the induction of cytokine release. *J Immunol.* (2005) 174:6518–23. doi: 10.4049/jimmunol.174.10.6518
13. van Heel DA, Ghosh S, Butler M, Hunt KA, Lundberg AM, Ahmad T, et al. Muramyl dipeptide and toll-like receptor sensitivity in NOD2-associated Crohn's disease. *Lancet.* (2005) 365:1794–6. doi: 10.1016/S0140-6736(05)66582-8
14. O'Neill LA, Kishon RJ, Rathmell J. A guide to immunometabolism for immunologists. *Nat Rev Immunol.* (2016) 16:553–65. doi: 10.1038/nri.2016.70
15. O'Neill LA, Pearce EJ. Immunometabolism governs dendritic cell and macrophage function. *J Exp Med.* (2016) 213:15–23. doi: 10.1084/jem.20151570
16. Reyes-Turcu FE, Ventii KH, Wilkinson KD. Regulation and cellular roles of ubiquitin-specific deubiquitinating enzymes. *Ann Rev Biochem.* (2009) 78:363–97. doi: 10.1146/annurev.biochem.78.082307.091526
17. Ashkenazi A, Bento CF, Ricketts T, Vicinanza M, Siddiqi F, Pavel M, et al. Polyglutamine tracts regulate beclin 1-dependent autophagy. *Nature.* (2017) 545:108–11. doi: 10.1080/15548627.2017.1336278
18. Kawaguchi Y, Okamoto T, Taniwaki M, Aizawa M, Inoue M, Katayama S, et al. CAG expansions in a novel gene for Machado-Joseph disease at chromosome 14q32.1. *Nat Genet.* (1994) 8:221–8. doi: 10.1038/ng1194-221
19. Paulson H. Machado-Joseph disease/spinocerebellar ataxia type 3. *Handb Clin Neurol.* (2012) 103:437–49. doi: 10.1016/B978-0-444-51892-7.00027-9
20. Kobayashi K, Inohara N, Hernandez LD, Galán JE, Núñez G, Janeway CA, et al. RICK/Rip2/CARDIAK mediates signalling for receptors of the innate and adaptive immune systems. *Nature.* (2002) 416:194–9. doi: 10.1038/416194a
21. Hasegawa M, Fujimoto Y, Lucas PC, Nakano H, Fukase K, Núñez G, et al. A critical role of RICK/RIP2 polyubiquitination in Nod-induced NF-kappaB activation. *EMBO J.* (2008) 27:373–83. doi: 10.1038/sj.emboj.7601962
22. Canning P, Ruan Q, Schwerdt T, Hrdinka M, Maki JL, Saleh D, et al. Inflammatory signaling by NOD-RIPK2 is inhibited by clinically relevant type II kinase inhibitors. *Chem Biol.* (2015) 22:1174–84. doi: 10.1016/j.chembiol.2015.07.017
23. Kawasaki T, Kawai T. Toll-like receptor signaling pathways. *Front Immunol.* (2014) 5:461. doi: 10.3389/fimmu.2014.00461
24. Kapoor A, Fan YH, Arav-Boger R. Bacterial Muramyl Dipeptide (MDP) restricts human cytomegalovirus replication via an IFN-beta-dependent pathway. *Scient Rep.* (2016) 6:20295. doi: 10.1038/srep20295
25. Xu J, Jiang C, Zhu W, Wang B, Yan J, Min Z, et al. NOD2 pathway via RIPK2 and TBK1 is involved in the aberrant catabolism induced by T-2 toxin in chondrocytes. *Osteoarthr Cartilage.* (2015) 23:1575–85. doi: 10.1016/j.joca.2015.04.016
26. Wild P, Farhan H, McEwan DG, Wagner S, Rogov VV, Brady NR, et al. Phosphorylation of the autophagy receptor optineurin restricts Salmonella growth. *Science.* (2011) 333:228–33. doi: 10.1126/science.1205405
27. Matsumoto G, Shimogori T, Hattori N, Nukina N. TBK1 controls autophagosomal engulfment of polyubiquitinated mitochondria through p62/SQSTM1 phosphorylation. *Hum Mol Genet.* (2015) 24:4429–42. doi: 10.1093/hmg/ddv179
28. Hornbeck PV, Zhang B, Murray B, Kornhauser JM, Latham V, Skrzypek E, et al. PhosphoSitePlus, 2014: mutations, PTMs and recalibrations. *Nucleic Acids Res.* (2015) 43:D512–20. doi: 10.1093/nar/gku1267
29. Niu S, Wang Z, Ge D, Zhang G, Li Y. Prediction of functional phosphorylation sites by incorporating evolutionary information. *Protein Cell.* (2012) 3:675–90. doi: 10.1007/s13238-012-2048-z
30. Mao Y, Senic-Matuglia F, Di Fiore PP, Polo S, Hodsdon ME, De Camilli P. Deubiquitinating function of ataxin-3: insights from the solution structure of the Josephin domain. *Proc Natl Acad Sci USA.* (2005) 102:12700–5. doi: 10.1073/pnas.0506344102
31. Harner M, Körner C, Walther D, Mokranjac D, Kaesmacher J, Welsch U, et al. The mitochondrial contact site complex, a determinant of mitochondrial architecture. *EMBO J.* (2011) 30:4356–70. doi: 10.1038/emboj.2011.379
32. von der Malsburg K, Müller JM, Bohnert M, Oeljeklaus S, Kwiatkowska P, Becker T, et al. Dual role of mitofilin in mitochondrial membrane organization and protein biogenesis. *Dev Cell.* (2011) 21:694–707. doi: 10.1016/j.devcel.2011.08.026
33. Bohnert M, Wenz LS, Zerbes RM, Horvath SE, Stroud DA, von der Malsburg K, et al. Role of mitochondrial inner membrane organizing system in protein biogenesis of the mitochondrial outer membrane. *Mol Biol Cell.* (2012) 23:3948–56. doi: 10.1091/mbc.e12-04-0295
34. Li H, Ruan Y, Zhang K, Jian F, Hu C, Miao L, et al. Mic60/Mitofilin determines MICOS assembly essential for mitochondrial dynamics and mtDNA nucleoid organization. *Cell Death Differ.* (2016) 23:380–92. doi: 10.1038/cdd.2015.102
35. Yang RF, Sun LH, Zhang R, Zhang Y, Luo YX, Zheng W, et al. Suppression of Mic60 compromises mitochondrial transcription and oxidative phosphorylation. *Scient Rep.* (2015) 5:7990. doi: 10.1038/srep07990
36. Rebelo AP, Dillon LM, Moraes CT. Mitochondrial DNA transcription regulation and nucleoid organization. *J Inher Metab Dis.* (2011) 34:941–51. doi: 10.1007/s10545-011-9330-8
37. Krawczyk CM, Holowka T, Sun J, Blagih J, Amiel E, DeBerardinis RJ, et al. Toll-like receptor-induced changes in glycolytic metabolism regulate dendritic cell activation. *Blood.* (2010) 115:4742–9. doi: 10.1182/blood-2009-10-249540
38. Murphy MP. How mitochondria produce reactive oxygen species. *Biochem J.* (2009) 417:1–13. doi: 10.1042/BJ20081386
39. West AP, Brodsky IE, Rahner C, Woo DK, Erdjument-Bromage H, Tempst P, et al. TLR signalling augments macrophage bactericidal activity through mitochondrial ROS. *Nature.* (2011) 472:476–80. doi: 10.1038/nature09973
40. Shiloh MU, MacMicking JD, Nicholson S, Brause JE, Potter S, Marino M, et al. Phenotype of mice and macrophages deficient in both phagocyte oxidase and inducible nitric oxide synthase. *Immunity.* (1999) 10:29–38. doi: 10.1016/S1074-7613(00)80004-7
41. Azkargorta M, Escobes I, Elortza F, Matthiesen R, Rodriguez MS. TUBES-mass spectrometry for identification and analysis of the ubiquitin-proteome. *Methods Mol Biol.* (2016) 1449:177–92. doi: 10.1007/978-1-4939-3756-1_9
42. Hjerpe R, Aillet F, Lopitz-Otsoa F, Lang V, England P, Rodriguez MS. Efficient protection and isolation of ubiquitylated proteins using tandem ubiquitin-binding entities. *EMBO Rep.* (2009) 10:1250–8. doi: 10.1038/embor.2009.192
43. Xolalpa W, Mata-Cantero L, Aillet F, Rodriguez MS. Isolation of the ubiquitin-proteome from tumor cell lines and primary cells using TUBES. *Proteostasis.* (2016) 1449:161–75. doi: 10.1007/978-1-4939-3756-1_8
44. Winborn BJ, Travis SM, Todi SV, Scaglione KM, Xu P, Williams AJ, et al. The deubiquitinating enzyme ataxin-3, a polyglutamine disease protein, edits Lys63 linkages in mixed linkage ubiquitin chains. *J Biol Chem.* (2008) 283:26436–43. doi: 10.1074/jbc.M803692200
45. Halligan DN, Murphy SJ, Taylor CT. The hypoxia-inducible factor (HIF) couples immunity with metabolism. *Semin Immunol.* (2016) 28:469–77. doi: 10.1016/j.smim.2016.09.004
46. Palazon A, Goldrath AW, Nizet V, Johnson RS. HIF transcription factors, inflammation, and immunity. *Immunity.* (2014) 41:518–28. doi: 10.1016/j.immuni.2014.09.008
47. Cramer T, Johnson RS. A novel role for the hypoxia inducible transcription factor HIF-1alpha: critical regulation of inflammatory cell function. *Cell Cycle.* (2003) 2:192–3. doi: 10.4161/cc.2.3.402
48. Peyssonnaud C, Cejudo-Martin P, Doedens A, Zinkernagel AS, Johnson RS, Nizet V. Cutting edge: essential role of hypoxia inducible factor-1alpha

- in development of lipopolysaccharide-induced sepsis. *J Immunol.* (2007) 178:7516–9. doi: 10.4049/jimmunol.178.12.7516
49. Peyssonnaud C, Datta V, Cramer T, Doedens A, Theodorakis EA, Gallo RL, et al. HIF-1 α expression regulates the bactericidal capacity of phagocytes. *J Clin Invest.* (2005) 115:1806–15. doi: 10.1172/JCI23865
 50. Gavin AL, Huang D, Huber C, Mårtensson A, Tardif V, Skog PD, et al. PLD3 and PLD4 are single-stranded acid exonucleases that regulate endosomal nucleic-acid sensing. *Nat Immunol.* (2018) 19:942–53. doi: 10.1038/s41590-018-0179-y
 51. Cruchaga C, Karch CM, Jin SC, Benitez BA, Cai Y, Guerreiro R, et al. Rare coding variants in the phospholipase D3 gene confer risk for Alzheimer's disease. *Nature.* (2014) 505:550–4. doi: 10.1038/nature12825
 52. Nibbeling EAR, Duarri A, Verschuuren-Bemelmans CC, Fokkens MR, Karjalainen JM, Smeets CJLM, et al. Exome sequencing and network analysis identifies shared mechanisms underlying spinocerebellar ataxia. *Brain.* (2017) 140:2860–78. doi: 10.1093/brain/awx251
 53. Heneka MT, Kummer MP, Latz E. Innate immune activation in neurodegenerative disease. *Nat Rev Immunol.* (2014) 14:463–77. doi: 10.1038/nri3705
 54. Sancak Y, Bar-Peled L, Zoncu R, Markhard AL, Nada S, Sabatini DM. Ragulator-rag complex targets mTORC1 to the lysosomal surface and is necessary for its activation by amino acids. *Cell.* (2010) 141:290–303. doi: 10.1016/j.cell.2010.02.024
 55. Takahashi Y, Nada S, Mori S, Soma-Nagae T, Oneyama C, Okada M. The late endosome/lysosome-anchored p18-mTORC1 pathway controls terminal maturation of lysosomes. *Biochem Biophys Res Commun.* (2012) 417:1151–7. doi: 10.1016/j.bbrc.2011.12.082
 56. Kimura T, Nada S, Takegahara N, Okuno T, Nojima S, Kang S, et al. Polarization of M2 macrophages requires Lamtor1 that integrates cytokine and amino-acid signals. *Nat Commun.* (2016) 7:13130. doi: 10.1038/ncomms13130
 57. Swatek KN, Komander D. Ubiquitin modifications. *Cell Res.* (2016) 26:399–422. doi: 10.1038/cr.2016.39
 58. Uhlén M, Fagerberg L, Hallström BM, Lindskog C, Oksvold P, Mardinoglu A. Proteomics. Tissue-based map of the human proteome. *Science.* (2015) 347:1260419. doi: 10.1126/science.1260419
 59. Nicastro G, Menon RP, Masino L, Knowles PP, McDonald NQ, Pastore A. The solution structure of the Josephin domain of ataxin-3: structural determinants for molecular recognition. *Proc Natl Acad Sci USA.* (2005) 102:10493–8. doi: 10.1073/pnas.0501732102
 60. Nicastro G, Masino L, Esposito V, Menon RP, De Simone A, Fraternali F, et al. Josephin domain of ataxin-3 contains two distinct ubiquitin-binding sites. *Biopolymers.* (2009) 91:1203–14. doi: 10.1002/bip.21210
 61. Evers MM, Toonen LJ, van Roon-Mom WM. Ataxin-3 protein and RNA toxicity in spinocerebellar ataxia type 3: current insights and emerging therapeutic strategies. *Mol Neurobiol.* (2014) 49:1513–31. doi: 10.1007/s12035-013-8596-2
 62. Chatterjee A, Saha S, Chakraborty A, Silva-Fernandes A, Mandal SM, Neves-Carvalho A, et al. The role of the mammalian DNA end-processing enzyme polynucleotide kinase 3'-phosphatase in spinocerebellar ataxia type 3 pathogenesis. *PLoS Genet.* (2015) 11:e1004749. doi: 10.1371/journal.pgen.1004749
 63. Gao R, Liu Y, Silva-Fernandes A, Fang X, Paulucci-Holthausen A, Chatterjee A, et al. Inactivation of PNKP by mutant ATXN3 triggers apoptosis by activating the DNA damage-response pathway in SCA3. *PLoS Genet.* (2015) 11:e1004834. doi: 10.1371/journal.pgen.1004834
 64. Li F, Macfarlan T, Pittman RN, Chakravarti D. Ataxin-3 is a histone-binding protein with two independent transcriptional corepressor activities. *J Biol Chem.* (2002) 277:45004–12. doi: 10.1074/jbc.M205259200
 65. Zhong X, Pittman RN. Ataxin-3 binds VCP/p97 and regulates retrotranslocation of ERAD substrates. *Hum Mol Genet.* (2006) 15:2409–20. doi: 10.1093/hmg/ddl164
 66. Burnett BG, Pittman RN. The polyglutamine neurodegenerative protein ataxin 3 regulates aggresome formation. *Proc Natl Acad Sci USA.* (2005) 102:4330–5. doi: 10.1073/pnas.0407252102
 67. Feng Q, Miao Y, Ge J, Yuan Y, Zuo Y, Qian L, et al. ATXN3 positively regulates type I IFN antiviral response by deubiquitinating and stabilizing HDAC3. *J Immunol.* (2018) 201:675–87. doi: 10.4049/jimmunol.1800285
 68. Yadava N, Nicholls DG. Spare respiratory capacity rather than oxidative stress regulates glutamate excitotoxicity after partial respiratory inhibition of mitochondrial complex I with rotenone. *J Neurosci.* (2007) 27:7310–7. doi: 10.1523/JNEUROSCI.0212-07.2007
 69. Ferrick DA, Neilson A, Beeson C. Advances in measuring cellular bioenergetics using extracellular flux. *Drug Discov Today.* (2008) 13:268–74. doi: 10.1016/j.drudis.2007.12.008
 70. van der Windt GJ, Everts B, Chang CH, Curtis JD, Freitas TC, Amiel E, et al. Mitochondrial respiratory capacity is a critical regulator of CD8(+) T cell memory development. *Immunity.* (2012) 36:68–78. doi: 10.1016/j.immuni.2011.12.007
 71. Garaude J, Acín-Pérez R, Martínez-Cano S, Enamorado M, Ugolini M, Nistal-Villán E, et al. Mitochondrial respiratory-chain adaptations in macrophages contribute to antibacterial host defense. *Nat Immunol.* (2016) 17:1037–45. doi: 10.1038/ni.3509
 72. Huang SC, Everts B, Ivanova Y, O'Sullivan D, Nascimento M, Smith AM, et al. Cell-intrinsic lysosomal lipolysis is essential for alternative activation of macrophages. *Nat Immunol.* (2014) 15:846–55. doi: 10.1038/ni.2956
 73. Kim W, Bennett EJ, Huttlin EL, Guo A, Li J, Possemato A, et al. Systematic and quantitative assessment of the ubiquitin-modified proteome. *Mol Cell.* (2011) 44:325–40. doi: 10.1016/j.molcel.2011.08.025
 74. Hu H, Sun SC. Ubiquitin signaling in immune responses. *Cell Res.* (2016) 26:457–83. doi: 10.1038/cr.2016.40
 75. Cramer T, Yamanishi Y, Clausen BE, Förster I, Pawlinski R, Mackman N, et al. HIF-1 α is essential for myeloid cell-mediated inflammation. *Cell.* (2003) 112:645–57. doi: 10.1016/S0092-8674(03)00154-5
 76. Nada S, Hondo A, Kasai A, Koike M, Saito K, Uchiyama Y, et al. The novel lipid raft adaptor p18 controls endosome dynamics by anchoring the MEK-ERK pathway to late endosomes. *EMBO J.* (2009) 28:477–89. doi: 10.1038/emboj.2008.308
 77. Guillaumot P, Luquin C, Malek M, Huber AL, Brugière S, Garin J, et al. Pdpr, a protein associated with late endosomes and lysosomes and implicated in cellular cholesterol homeostasis. *PLoS ONE.* (2010) 5:e10977. doi: 10.1371/journal.pone.0010977
 78. Zoncu R, Bar-Peled L, Efeyan A, Wang S, Sancak Y, Sabatini DM. mTORC1 senses lysosomal amino acids through an inside-out mechanism that requires the vacuolar H(+)-ATPase. *Science.* (2011) 334:678–83. doi: 10.1126/science.1207056
 79. Bar-Peled L, Schweitzer LD, Zoncu R, Sabatini DM. Ragulator is a GEF for the rag GTPases that signal amino acid levels to mTORC1. *Cell.* (2012) 150:1196–208. doi: 10.1016/j.cell.2012.07.032
 80. Zhang CS, Jiang B, Li M, Zhu M, Peng Y, Zhang YL, et al. The lysosomal v-ATPase-ragulator complex is a common activator for AMPK and mTORC1, acting as a switch between catabolism and anabolism. *Cell Metab.* (2014) 20:526–40. doi: 10.1016/j.cmet.2014.06.014
 81. Wu C, Orozco C, Boyer J, Leglise M, Goodale J, Batalov S, et al. BioGPS: an extensible and customizable portal for querying and organizing gene annotation resources. *Genome Biol.* (2009) 10:R130. doi: 10.1186/gb-2009-10-11-r130
 82. Corridoni D, Arseneau KO, Cifone MG, Cominelli F. The dual role of nod-like receptors in mucosal innate immunity and chronic intestinal inflammation. *Front Immunol.* (2014) 5:317. doi: 10.3389/fimmu.2014.00317
 83. Davis S, Charles PD, He L, Mowlds P, Kessler BM, Fischer R. Expanding proteome coverage with charge ordered parallel ion analysis (CHOPIN) combined with broad specificity proteolysis. *J Prot Res.* (2017) 16:1288–99. doi: 10.1021/acs.jproteome.6b00915

Conflict of Interest Statement: The authors declare that the research was conducted in the absence of any commercial or financial relationships that could be construed as a potential conflict of interest.

Copyright © 2019 Chapman, Corridoni, Shiraishi, Pandey, Aulicino, Wigfield, do Carmo Costa, Thézénas, Paulson, Fischer, Kessler and Simmons. This is an open-access article distributed under the terms of the Creative Commons Attribution License (CC BY). The use, distribution or reproduction in other forums is permitted, provided the original author(s) and the copyright owner(s) are credited and that the original publication in this journal is cited, in accordance with accepted academic practice. No use, distribution or reproduction is permitted which does not comply with these terms.